ISTANBUL TECHNICAL UNIVERSITY ★ GRADUATE SCHOOL

UNDERSTANDING OF POLARIZATION AND SPIN CORRELATION OF TOP QUARK PAIRS FOR PRECISION MEASUREMENTS AND NEW PHYSICS SEARCHES

M.Sc. THESIS

Orçun KOLAY

Department of Physics Engineering

Physics Engineering Programme

JULY 2021

ISTANBUL TECHNICAL UNIVERSITY ★ GRADUATE SCHOOL

UNDERSTANDING OF POLARIZATION AND SPIN CORRELATION OF TOP QUARK PAIRS FOR PRECISION MEASUREMENTS AND NEW PHYSICS SEARCHES

M.Sc. THESIS

Orçun KOLAY
(509181115)

Department of Physics Engineering

Physics Engineering Programme

Thesis Advisor: Prof. Dr. M. Altan ÇAKIR

JULY 2021

İSTANBUL TEKNİK ÜNİVERSİTESİ ★ LİSANSÜSTÜ EĞİTİM ENSTİTÜSÜ

HASSASLIK ÖLÇÜMLERİ VE YENİ FİZİK ARAŞTIRMALARI İÇİN ÜST KUARK ÇİFTLERİNİN POLARİZASYONU VE SPİN KORELASYONUNUN ANLAŞILMASI

YÜKSEK LİSANS TEZİ

Orçun KOLAY
(509181115)

Fizik Mühendisliği Anabilim Dalı

Fizik Mühendisliği Programı

Tez Danışmanı: Prof. Dr. M. Altan ÇAKIR

TEMMUZ 2021

Orçun KOLAY, a M.Sc. student of ITU Graduate School with student ID 509181115, successfully defended the thesis entitled "UNDERSTANDING OF POLARIZATION AND SPIN CORRELATION OF TOP QUARK PAIRS FOR PRECISION MEASUREMENTS AND NEW PHYSICS SEARCHES", which he prepared after fulfilling the requirements specified in the associated legislations, before the jury whose signatures are below.

Thesis Advisor :	**Prof. Dr. M. Altan ÇAKIR** Istanbul Technical University	.....
Jury Members :	**Prof. Dr. Cenap Şahabettin ÖZBEN** Istanbul Technical University	.....
	Prof. Dr. Altuğ ÖZPİNECİ Middle East Technical University	.....

Date of Submission : 11 June 2021
Date of Defense : 9 July 2021

To my family,

FOREWORD

Firstly, I would like to express my sincere gratitude to my supervisor Prof. Dr. M. Altan Çakır for his excellent guidance in instilling a research mentality, his motivation and his friendship. I am also thankful to the rest of my thesis committee: Prof. Dr. Cenap Şahabettin Özben and Prof. Dr. Altuğ Özpineci for accepting to be a member of my jury.

In addition, I would like to thank the Scientific and Technological Research Council of Turkey (TUBITAK) for financial support under 2210-A National Scholarship Programme for MSc Students during my master's study.

July 2021 Orçun KOLAY

TABLE OF CONTENTS

Page

FOREWORD ..... **ix**
TABLE OF CONTENTS ..... **xi**
ABBREVIATIONS ..... **xiii**
SYMBOLS ..... **xv**
LIST OF TABLES ..... **xvii**
LIST OF FIGURES ..... **xix**
SUMMARY ..... **xxiii**
ÖZET ..... **xxv**
1. INTRODUCTION TO STANDARD MODEL **1**
1.1 Standard Model of Elementary Particle Physics 1
1.1.1 Top quark 5
1.2 Beyond the Standard Model 6
1.2.1 Top quark in BSM searches 7
1.3 The Large Hadron Collider Experiment 10
2. MONTE CARLO EVENT GENERATORS IN PARTICLE PHYSICS **11**
2.1 Theoretical Foundation of Event Generation 11
2.2 Steps in the Generation of the Events 14
2.2.1 Hard process 15
2.2.2 Parton shower 17
2.2.3 Matching and merging 18
2.2.4 Fragmentation and hadronization 19
2.2.5 Underlying events 20
2.3 Fast Detector Simulation 20
3. SPIN CORRELATION AND POLARIZATION FOR TOP QUARK PAIRS AT THE LHC **21**
3.1 Analysis and Computational Setup 21
3.1.1 Analysis flow 21
3.1.2 Monte Carlo data samples 22
3.2 The Formalism of the Spin Density Matrix 25
4. RESULTS AND INTERPRETATION **31**
4.1 Theory-Data Comparison Analysis 31
4.2 Implications of Precision Measurements of Beyond the Standard Model 37
5. CONCLUSION AND OUTLOOK **45**
REFERENCES **49**
APPENDICES **55**
APPENDIX A 57
APPENDIX B 65
CURRICULUM VITAE **71**

ABBREVIATIONS

ALICE	**:** A Large Ion Collider Experiment
ATLAS	**:** A Toroidal LHC Apparatus
BSM	**:** Beyond Standard Model
CERN	**:** European Organisation for Nuclear Research
CDF	**:** Collider Detector at Fermilab
CKM	**:** Cabibbo–Kobayashi–Maskawa
CMS	**:** Compact Muon Solenoid
DM	**:** Dark Matter
FSR	**:** Final-State Radiation
HL-LHC	**:** High-Luminosity LHC
ISR	**:** Initial-State Radiation
LHC	**:** Large Hadron Collider
LHCb	**:** Large Hadron Collider beauty
LO	**:** Leading Order
LSP	**:** Lightest Supersymmetric Particle
MC	**:** Monte Carlo
ME	**:** Matrix Element
NLO	**:** Next-to Leading Order
NNLO	**:** Next-to-Next-to Leading Order
PDF	**:** Parton Distribution Function
PS	**:** Parton Shower
QCD	**:** Quantum Chromodynamics
QED	**:** Quantum Electrodynamics
SM	**:** Standard Model
SUSY	**:** Supersymmetry

SYMBOLS

$\mathbf{E}_T^{miss}$	**:** Missing Transverse Energy
$\mathbf{P}_T$	**:** Transverse Momentum

LIST OF TABLES

Page

Table 1.1 : The SM fermions are illustrated with the associated quantum numbers. **4**

Table 3.1 : Matrix Element (ME) event generator settings for $t\bar{t}$ and BSM signal samples used in this study. The generator versions, the order of QCD accuracy of associated predictions, the PDF sets used in ME calculations and the merging scheme are shown. **23**

Table 3.2 : Observable quantities of the spin density matrix and their corresponding measured coefficients, coefficient functions and P and CP symmetry properties. **29**

LIST OF FIGURES

Page

Figure 1.1 : Elementary particles in the SM: all fermions and bosons are specified with their mass, electric charge and spin. Interaction relations between fermions and bosons are demonstrated with grey loops. **2**

Figure 1.2 : A diagram indicating interactions between fundamental particles in the SM [1]. **3**

Figure 1.3 : A representation of SM particles and their SUSY superpartners. **8**

Figure 1.4a: SUSY signal. **9**

Figure 1.4b: Dark matter signal. **9**

Figure 1.4c: RPV SUSY signal. **9**

Figure 1.4 : Diagrams of the signal samples. **9**

Figure 2.1 : A tree-level Feynman diagram of the $(e^+e^- \to \mu^+\mu^-)$ scattering process [2]. **12**

Figure 2.2 : The lowest order Feynman diagrams for top quark pair production [3]. **13**

Figure 2.3 : The structure of a $t\bar{t}h$ event generated by an event generator. All separate steps are represented by different colors: the hard process in red, hadronization in light green, hadron decay in dark green, underlying events in purple and photon radiation in yellow [4]. **15**

Figure 2.4 : Schematic representation of the cluster (left) and the string (right) models [5]. **19**

Figure 3.1 : A representative flowchart of the analysis. **22**

Figure 3.2 : Coordinate system illustrating t and $\bar{t}$ helicity spin basis. The $\hat{k}$ axis is described as the direction of flight of top quark measured in the $t\bar{t}$ CM. The directions $\hat{k}$, $\hat{r}$, $\hat{p}$ and $\bar{t}$ are in the scattering plane which the normal is the direction $\hat{n}$. The signs of the $\hat{r}$ and $\hat{n}$ axes can have inverse according to the angle Θ as shown in equation (3.5). The angles between the direction of flight of the positively ℓ^+ (negatively ℓ^-) charged lepton in the top quark (anti-quark) rest frame and the axes $\hat{a}$ ($\hat{b}$) determined in equation (3.5) are used to calculate the coefficients in equations (3.9)-(3.12). . **28**

Figure 4.1 : The normalized differential cross sections with respect to the diagonal spin correlation observables $\cos\theta_1^i \cos\theta_2^i$, $i = k,r,n$ compared to the CMS data and the predictions from MADGRAPH5_aMC@NLO, SHERPA and POWHEG BOX in full phase space. The ratio of the normalized differential cross sections predicted by the other generator+parton shower configurations to MADGRAPH5+PYTHIA8 at NLO is shown in the lower panels. The statistical uncertainty band is shown in grey. The yellow uncertainty bands represent the overall uncertainty obtained by summing the systematic and statistical uncertainties in quadrature. The systematic uncertainty includes PDF and scale uncertainties. **33**

Figure 4.2 : The normalized differential cross sections with respect to the cross spin correlation observables $\cos\theta_1^i \cos\theta_2^j \pm \cos\theta_1^j \cos\theta_2^i$, $i \neq j$. The ratio panels compare the other predictions to nominal distribution. **34**

Figure 4.3 : The normalized differential cross sections with respect to the observables $\cos\theta_1^i$ and $\cos\theta_2^i$, $i = k,r,n$. The ratio panels compare the other predictions to nominal distribution. **35**

Figure 4.4 : The normalized differential cross sections with respect to the observables $\cos\theta_1^{i*}$ and $\cos\theta_2^{i*}$, $i = k,r,n$. The ratio panels compare the other predictions to nominal distribution. **36**

Figure 4.5 : The normalized differential cross section as a function of laboratory frame observable which are $|\Delta\phi_{ll}|$ (left plot) and $\cos\varphi_{lab}$ (right plot). The ratio panels compare the other predictions to nominal distribution. **37**

Figure 4.6 : The normalized differential cross section with respect to $\cos\varphi$ predicted by various MC event generators at LO, NLO and NLO-EW accuracy. The ratio of the other predictions to nominal distribution is shown in the lower panel. **38**

Figure 4.7 : The normalized differential cross sections with respect to the diagonal spin correlation observables $\cos\theta_1^i \cos\theta_2^i$, $i = k,r,n$ compared to the nominal $t\bar{t}$ sample, the CMS data and the BSM signals. The statistical uncertainty band of the SM $t\bar{t}$ samples is shown in grey. The yellow uncertainty bands represent the overall uncertainty obtained by summing the systematic and statistical uncertainties of the SM $t\bar{t}$ samples in quadrature. The statistical uncertainties of the signals are specified on each signal sample. **39**

Figure 4.8 : The normalized differential cross sections with respect to the cross spin correlation observables $\cos\theta_1^i \cos\theta_2^j \pm \cos\theta_1^j \cos\theta_2^i$, $i \neq j$. The ratio panels compare the BSM signals to the nominal distribution. **41**

Figure 4.9 : The normalized differential cross sections with respect to the observables $\cos\theta_1^i$ and $\cos\theta_2^i$, $i = k,r,n$. The ratio panels compare the BSM signals to the nominal distribution. **42**

Figure 4.10: The normalized differential cross sections with respect to the observables $\cos\theta_1^{i*}$ and $\cos\theta_2^{i*}$, $i = k,r,n$. The ratio panels compare the BSM signals to the nominal distribution. **43**

Figure 4.11: The normalized differential cross section as a function of laboratory frame observable which are $|\Delta\phi_{ll}|$ (left plot) and $\cos\varphi_{lab}$ (right plot).The ratio panels compare the BSM signals to the nominal distribution. **43**

Figure 4.12: The normalized differential cross section with respect to $\cos\varphi$. The ratio panel compares the BSM signals to the nominal distribution. **44**

Figure B.1 : The normalized differential cross sections with respect to the diagonal spin correlation observables $\cos\theta_1^i\cos\theta_2^i$, $i = k,r,n$ compared to the nominal $t\bar{t}$ sample, the CMS data and the RPV SUSY signals with different stop $\tilde{t}$ masses. The ratio panels compare the RPV SUSY signals to the nominal distribution. **65**

Figure B.2 : The normalized differential cross sections with respect to the cross spin correlation observables $\cos\theta_1^i\cos\theta_2^j \pm \cos\theta_1^j\cos\theta_2^i$, $i \neq j$. The ratio panels compare the RPV SUSY signals to the nominal distribution. **66**

Figure B.3 : The normalized differential cross sections with respect to the observables $\cos\theta_1^i$ and $\cos\theta_2^i$, $i = k,r,n$. The ratio panels compare the RPV SUSY signals to the nominal distribution. **67**

Figure B.4 : The normalized differential cross sections with respect to the observables $\cos\theta_1^{i*}$ and $\cos\theta_2^{i*}$, $i = k,r,n$. The ratio panels compare the RPV SUSY signals to the nominal distribution. **68**

Figure B.5 : The normalized differential cross section as a function of laboratory frame observable which are $|\Delta\phi_{ll}|$ (left plot) and $\cos\varphi_{lab}$ (right plot).The ratio panels compare the RPV SUSY signals to the nominal distribution. **68**

Figure B.6 : The normalized differential cross section with respect to $\cos\varphi$. The ratio panel compares the RPV SUSY signals to the nominal distribution. **69**

UNDERSTANDING OF POLARIZATION AND SPIN CORRELATION OF TOP QUARK PAIRS FOR PRECISION MEASUREMENTS AND NEW PHYSICS SEARCHES

SUMMARY

The standard model (SM) is a powerful theory that describes the three interactions, except gravity, with all other elementary particles. It has been tested in many experiments so far and has been successful in its predictions. The most advanced of these experiments is the Large Hadron Collider (LHC) at the European Organization for Nuclear Research (CERN) in Geneva, Switzerland. The LHC played a major role in completing the Standard Model with the discovery of the Higgs boson.

The SM is not a theory that explains everything, although all the particles it predicts have been found. The hierarchy problem, dark matter, matter-antimatter asymmetry, and the unification of the fundamental interactions are the main problems that this model is not able to answer and still need to be solved. To solve these problems, physicists have developed other theories beyond the standard model (BSM) such as Supersymmetry (SUSY). SUSY establishes a symmetry between bosons and fermions by mentioning that each boson and fermion in the SM has a supersymmetric partner. Thus, SUSY is a model that many theory and experimental groups work on due to bring a solution to some problems in the SM.

As mentioned above, all particles predicted by the SM were observed. Among these particles, the particle with the heaviest mass is the top quark. With a mass of about 172.5 GeV, the top quark is about 40 times heavier than even the next heaviest quark. This remains an unexplained question in the SM. The massive mass of the top quark makes it play an important role in research beyond the standard model. The Yukawa coupling of the top quark is close to unity, making it the particle that interacts the most with the Higgs boson. Also, the Higgs boson mass gets a large level of quantum correction from its interaction with the top quark. All this causes the top quark to hold an important place in standard model precision measurements.

Precision measurements are needed to observe the difference of experiments from the standard model predictions and to support new theories with experiments. At this point, spin correlation and polarization of top quark pairs, which will be discussed in this thesis, gain importance. Due to its weight and very short lifetime, the top quarks produced in collision processes decay into other particles before hadronization. This allows the top quark, which is preserved from the effects of hadronization, to transmit its spin alignment information to its decay products. Due to their short lifetimes, top quarks are not observed in experiments, but leptons and hadronized quarks are detected. Based on these particles observed as the final product, it is possible to have information about spin of the top quark.

In this study, the case of two top quarks going into a full leptonic decay will be discussed. In the mathematical modeling of spin correlation and polarization, a total of 22 observables were dealt with by using the spin density matrix.

Monte Carlo event generators are critical tools in high energy physics calculations. They play a major role in the leading and next to leading order calculations, in QCD, but also in the electroweak corrections. Based on a high level of calculation, studied with LHC data, these contributions allow for both the realistic simulation of top quark pairs precision measurements and the possible understanding of BSM signals. While there are various Monte Carlo event generators, this study covers three: MADGRAPH5_aMC@NLO, SHERPA and POWHEG BOX. In addition, the parton shower technique, which makes predictions closer to reality, is also provided with PYTHIA.

In this thesis, it will be examined the behavior of the spin correlation and polarization observables of the above-mentioned top quark pairs under different Monte Carlo event generator approaches. With the help of Monte Carlo event generators, the effects of high order in QCD and electroweak corrections on spin correlations of top quarks were investigated. The effect of different Monte Carlo configurations on each element in the spin density matrix is discussed in detail. All the simulation results were compared with the experimental results of the CMS group.

The collision events mentioned in this thesis are the superpartner of the top quark (stop) pair production, decayed into a top quark and a lightest supersymmetric particle (LSP), and the top quark pair production associated with dark matter. These models have been studied by many groups so far. But, they were partially carried out in high missing transverse energy regions that can be studied more easily, and the most of the phase space of the stop quark mass is excluded at 95% confidence level. Recently, the focus has been on the low missing transverse energy region, which is partly difficult to study.

Within the reach of the thesis, it is aimed to contribute to the precision measurements with spin correlation and polarization observables in the low missing transverse energy regions of the above-mentioned models by means of different Monte Carlo estimations. In these models, for the low missing transverse energy region, that the difference between the stop and the LSP masses in the SUSY samples is slightly larger than the top quark, and in the dark matter samples, that the mediator mass is relatively small is chosen as a scenario. In addition, the R-Parity violating (RPV) SUSY model is also included in the study.

The thesis is structured as follows: A brief introduction to the standard model is given in Chapter 1. In addition, the problems in the Standard Model and the theories developed for their solution are mentioned and the Large Hadron Collider is introduced. The Monte Carlo event generators used in this study and the steps in the simulations of the collision events are explained in Chapter 2. In Chapter 3, the analysis method used in the study and the parameters of the samples used in Monte Carlo event generators are detailed. In addition, mathematical modeling of spin correlation and polarization in top quark pairs is discussed in this section. The results from the analysis are discussed in detail in Chapter 4. Finally, in Chapter 5, the analysis is with final remarks concluded and recommendations for further analysis are given.

HASSASLIK ÖLÇÜMLERİ VE YENİ FİZİK ARAŞTIRMALARI İÇİN ÜST KUARK ÇİFTLERİNİN POLARİZASYONU VE SPİN KORELASYONUNUN ANLAŞILMASI

ÖZET

İnsanlık doğayı daha iyi anlayabilmek için tarih boyunca çeşitli teoriler geliştirmiştir. Bu teoriler çağlar boyunca yapılan gözlemler ve matematiksel metotların gelişmesiyle üzerine koyularak günümüzdeki halini almıştır. Günlük dilimizde bile yer edinmiş atom kavramı çok eski zamanlara dayanmaktadır. Atomların ve atomların oluşturduğu karmaşık yapıların anlaşılmasından pek çok bilim dalı doğmuş olup bunların sonucunda da teknoloji müthiş bir ivmeyle gelişim göstermiştir. Son gelinen noktada atomik ölçeklerin de altında deneyler yapmak olağan bir durum olmuştur. Özellikle 20. yüzyılda kuantum devrimiyle birlikte atomun ve onu oluşturan bileşenlerin daha iyi anlaşılması yeni bir çağın başlangıcı olmuştur. P. A. M. Dirac'ın göreceli kuantum teorisi'nde bahsettiği pozitif yüklü elektronların olabileceği fikri parçacık fiziğinin en önemli yapı taşlarından olmuştur. Bununla birlikte bir çok yeni atom altı parçacık keşfedilmiş ve bunların kütle çekim, elektromanyetik, zayıf ve güçlü yeğin kuvvet olmak üzere farklı etkileşimlerde bulundukları anlaşılmıştır. Fizikçiler tüm bu karmaşıklığı Standart Model adı verilen bir teoride anlaşılır kılmaya çalışmışlardır.

Standart Model, kütle çekim dışında üç etkileşimi diğer bütün temel parçacıklarla birlikte tanımlayan güçlü bir teoridir. Şimdiye kadar bir çok deneyde test edilmiş ve öngörülerinde başarılı olmuştur. Bu deneylerin en gelişmiş olanı İsviçre'nin Cenevre kentinde bulunan Avrupa Nükleer Araştırmalar Merkezi'ndeki (CERN) Büyük Hadron Çarpıştırıcısıdır (Large Hadron Collider-LHC). Kompozit bir parçacık olan protonları çok yüksek hızlarda çarpıştırarak Standart Model'in test edilmesine olanak sağlamaktadır. Son olarak Higgs bozonunu keşfederek Standart Model'in tamamlanmasında büyük bir rol oynamıştır.

Standart Model, öngördüğü tüm parçacıklar bulunmuş olsa da her şeyi açıklayan bir teori değildir. Hiyerarşi problemi, karanlık madde, madde-karşıt madde asimetrisi, dört kuvvetin birleştirilememiş olması bu modelin çözüm getiremediği başlıca meselelerdir.

Bu sorunları çözmek için fizikçiler Standart Model'in ötesinde başka teoriler geliştirmişlerdir. Bunların arasında, deneysel olarak herhangi bir kanıt olmamasına rağmen Süpersimetri (Supersymmetry-SUSY) en çok kabul gören teori olmuştur. Standart Model'de bulunan her bir bozon ve fermiyona bir süpersimetrik eşlikçi olduğundan bahsederek bozonlar ve fermiyonlar arasında bir simetri kurmaktadır. Bununla birlikte SUSY yukarıda bahsedilen problemlerin bir çoğuna çözüm getirmektedir. Bundan dolayı bir çok teori ve deney grubunun üzerinde çalıştığı bir modeldir.

Yukarıda bahsedildiği gibi Standart Model'in öngördüğü tüm parçacıklar gözlemlenmiştir. Bu parçacıklar arasında en ağır kütleye sahip olan parçacık üst (top) kuarktır. Yaklaşık 172.5 GeV kütleye sahip olan üst kuark bir sonraki en ağır kuarktan bile yaklaşık 40 kat daha ağırdır. Bu da Standart Model'de açıklanmayan bir soru olarak durmaktadır. Üst kuarkın bu kadar fazla olan kütlesi onu Standart Model ötesi araştırmalarda önemli bir rol oynamasına neden olmaktadır. Üst kuarkın Yukawa bağlantısının bire yakın olması onu Higgs bozonu ile en çok etkileşime giren parçacık yapmaktadır. Ayrıca Higgs bozonu kütlesi üst kuark ile etkileşmesinden fazla miktarda kuantum düzeltmesi almaktadır. Tüm bunlar üst kuarkın Standart Model hassaslık ölçümlerinde önemli bir yer tutmasına neden olmaktadır.

Yukarıda bahsedildiği gibi Standart Model bazı sorulara bir açıklama getirememesine rağmen özellikle LHC çerçevesinde yapılan bir çok deneyden başarıyla çıkmıştır. Ama bilinen bir gerçek var ki Standart Model evreni tamamen açıklayan bir teori değildir. Bu sebeple deneylerin Standart Model'den farkının gözlemlenmesi ve yeni teorilerin deney ile desteklenmesi için hassaslık ölçümlerine ihtiyaç vardır. Bu noktada bu tezde de ele alınacak olan üst kuark çiftlerinin spin korelasyon ve polarizasyonları önem kazanmaktadır. Sahip olduğu ağırlığı ve çok kısa olan ömründen dolayı çarpışma işlemlerinde meydana gelmiş olan üst kuarklar hadronize olamadan başka parçacıklara bozunmaktadır. Bu da hadronizasyondan gelen etmenlerden korunmuş olan üst kuarkın spin hizalanma bilgisini bozunduğu parçacıklara aktarmasına olanak tanımaktadır. Kısa ömürlerinde dolayı deneylerde üst kuarklar gözlemlenmeyip leptonlar ve hadronize olmuş kuarklar tespit edilmektedir. Son ürün olarak gözlemlenen bu parçacıklardan yola çıkarak üst kuarkın spin bilgisi hakkında yorum yapılabilmektedir.

Protonların çarpışmasından gelen üst kuark çiftlerinin spin bilgisine yukarıda bahsedildiği gibi farklı parçacıklar yardımıyla ulaşılabilmektedir. Bu çalışmada iki üst kuarkın da lepton içeren bir bozunma gerçekleştirmesi durumu ele alınacaktır. Bunun sebepleri olarak her ne kadar tesir kesiti küçük olsa da hadronize olmuş kuarklara göre daha net momentum bilgisi elde edilmesi ve daha sonra bahsedilecek olan spin korelasyonu daha iyi aktarması gösterilebilir. Spin korelasyonun ve polarizasyonun matematiksel olarak modellenmesinde spin yoğunluk matrisinden faydalanılarak toplamda 22 tane gözlemlenebilir ile ilgilenilmiştir.

Yüksek enerji fiziği hesaplamalarında Monte Carlo olay üreteçleri çok sık kullanılan araçlardır. Kuantum renk dinamiğinde (QCD) pertürbatif bölgede ilk ve ikinci en büyük katkıların olduğu Feynman diyagramlarının hesaplanmasında büyük rol oynamaktadırlar. Buradan hareketle parçacık çarpıştırma olaylarının benzeşimlerinin yapılması ve bu olaylardan çok yüksek miktarlarda elde edilmesinde kullanılmaktadırlar. Deneylerden elde edilecek verilerin nasıl karakteristiklerinin olacağı bu araçlar sayesinde önceden kestirim yapılarak bulunmaktadır. Ayrıca yeni fizik modelleri de bu araçlar sayesinde deney sonuçları ile kıyaslanabilmektedir. Çeşitli Monte Carlo olay üreteçleri olmakla birlikte bu çalışmada üç tanesi ele alınmaktadır: MADGRAPH5_aMC@NLO, SHERPA and POWHEG BOX. Bunlara ek olarak benzeşim verisinin gerçeğe daha yakın olmasını sağlayan parton duşu tekniğin de PYTHIA ile sağlanmaktadır.

Bu tez, yukarıda bahsedilen üst kuark çiftlerinin spin korelasyon ve polarizasyon gözlemlenebilirlerinin farklı Monte Carlo olay üreteçleri yaklaşımları altında davranışlarını ele almaktadır. Monte Carlo olay üreteçleri yardımıyla QCD'de

yüksek mertebelerin ve elektro-zayıf düzeltmelerin üst kuarkların spin korelasyonları üzerindeki etkileri araştırılmıştır. Farklı Monte Carlo yapılandırmalarının spin yoğunluk matrisindeki her bir elemanın üzerindeki etkisi detaylı olarak ele alınmıştır. Tüm benzeşim sonuçları CMS grubunun deney sonuçları ile kıyaslanmıştır.

Farklı Monte Carlo olay üreteçlerinin üst kuark spin korelasyon gözlemlenebilirleri açısından farklılıklarının ortaya çıkarılmasına ek olarak ATLAS ve CMS başta olmak üzere çeşitli grupların üzerinde çalıştığı Standart Model ötesi modellerin bu gözlemlenebilirler ile testi gerçekleştirilmiştir. Bu tezde sözü geçen çarpışma olayları üst kuarkın süper partneri olan s-üst (stop) kuark çiftinin bir üst kuarka ve bir de neutralino'ya bozunması ve üst kuark çiftiyle ilişkili karanlık madde üretimidir. Bu modeller şimdiye kadar bir çok grup tarafından çalışılmıştır. Bu çalışmalar kısmen daha kolay üzerinde çalışılabilen yüksek kayıp enerji bölgelerinde yapılmış olup herhangi bir s-üst kuark ya da karanlık madde izine rastlanmamıştır. Son dönemde düşük kayıp enerji bölgelerinde çalışmalar yoğunlaşmış olup Standart Model ötesi bir parçacık izine rastlanmamasına rağmen bu bölge hala gizemini korumaktadır.

Tez kapsamında, yukarıda bahsedilen modellerin düşük kayıp enerjili bölgelerinde spin korelasyon ve polarizasyon gözlemlenebilirleri ile hassaslık ölçümlerine farklı Monte Carlo tahminleri aracılığıyla katkı sağlamak amaçlanmıştır. Bu modellerde düşük kayıp enerji bölgesine bakmak için SUSY örneklerinde s-üst (stop) ve neutralino kütleleri arasındaki farkın üst kuarktan biraz büyük, karanlık madde örneklerinde ise karanlık madde parçacıklarının oluşmasına aracılık eden parçacığın kütlesinin görece küçük olması senaryo olarak seçilmiştir. Ayrıca ayrık bir simetri olan R-Parity'nin korunmaması durumundaki SUSY örneği de çalışmaya dahil edilmiştir.

Tez şu şekilde yapılandırılmıştır: Bölüm 1'de Standart Model'e kısa bir giriş yapılmıştır. Standart Model'deki problemler ve bunların çözümü için geliştirilen teorilerden bahsedilmiş olup Büyük Hadron Çarpıştırıcısı tanıtılmıştır. Bu çalışmada kullanılan Monte Carlo olay üreteçleri ve bir çarpışma olayının hangi aşamalardan geçilerek benzeşim yapıldığı Bölüm 2'de anlatılmıştır. Bölüm 3'te, çalışmada kullanılan analiz yöntemi ve Monte Carlo olay üreteçlerinde kullanılan örneklerin parametreleri detaylandırılmıştır. Ayrıca üst kuark çiftlerinde spin korelasyon ve polarizasyonun matematiksel olarak modellenmesi bu bölümde ele alınmıştır. Analizden elde edilen sonuçlar Bölüm 4'te ayrıntılı bir şekilde tartışılmıştır. Son olarak Bölüm 5'te analizden elde edilen çıktılar sonuçlandırılmış ve sonraki analizler için öneriler verilmiştir.

1. INTRODUCTION TO STANDARD MODEL

1.1 Standard Model of Elementary Particle Physics

The standard model is a quantum field theory that describes elementary particles and how they interact with each other and it explains three of the four fundamental known forces which are electromagnetic, weak and strong interactions. All ordinary matter known in nature is described by the SM with a few elementary particles. In general, these particles can be categorized according to whether they have integer or half-integer spin. Accordingly, particles with half-integer spin are called fermions, while particles with integer spin are bosons. The other main difference between fermion and boson is that fermions obey the Pauli exclusion principle, which prevents two identical fermions from being in the same quantum state, whereas bosons do not have such a limitation. Matter particles are composed of quarks and leptons, which are also fermions. Leptons and quarks interact through electromagnetic, weak and strong forces in which bosons are the mediators of these forces. A summary of elementary particles and their interactions is shown in figure 1.1. Leptons consist of three different generations, with each generation containing a charged lepton (electron, muon and tau) and a neutral lepton (electron neutrino, muon neutrino and tau neutrino), so called neutrino. Likewise, quarks have three generations, but they also hold six different flavors (up quark, down quark, charm quark, strange quark, top quark, bottom quark). In addition, each lepton and quark have oppositely charged antiparticle that is the same in terms of mass and other quantum numbers.

In the case of leptons, charged leptons interact with the weak and electromagnetic force, while neutrinos obey only the weak interaction. This causes neutrinos to not be detected directly in the experiments. Quarks, on the other hand, interact with the strong force due to their color charged, as well as electromagnetic interaction.

As mentioned above, bosons are particles with integer spin and are responsible for the interactions between matter particles. As mentioned in the previous paragraph,

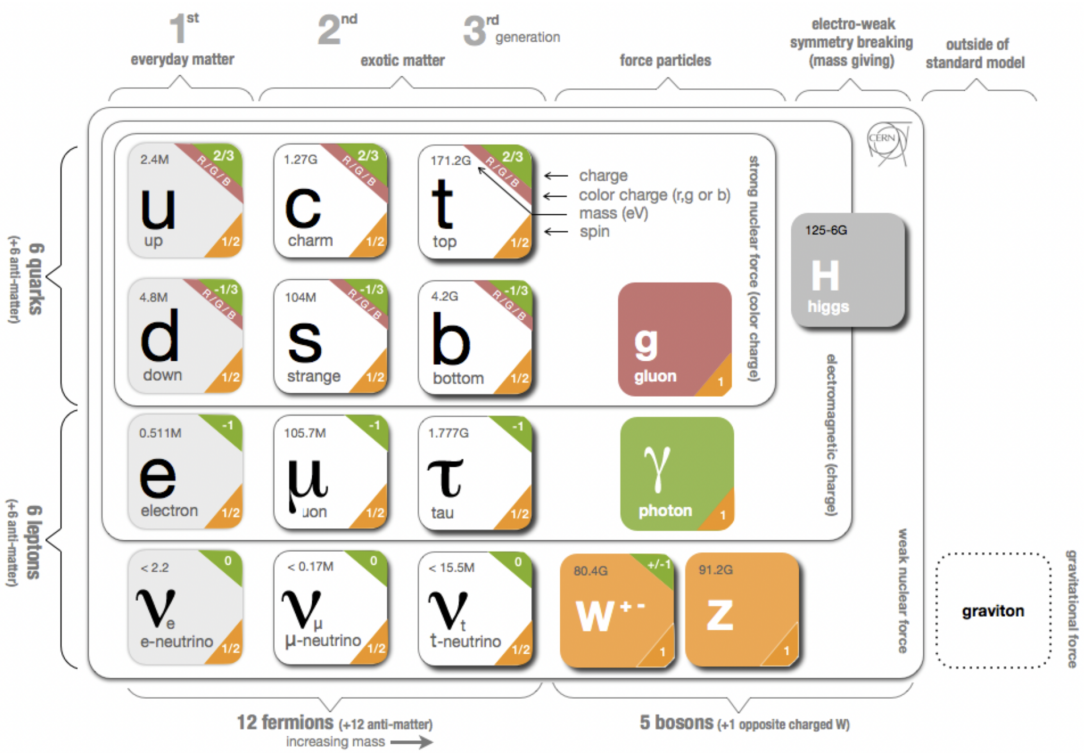

Figure 1.1 : Elementary particles in the SM: all fermions and bosons are specified with their mass, electric charge and spin. Interaction relations between fermions and bosons are demonstrated with grey loops.

leptons and quarks play a role in different interactions, and the carrier particles of these interactions are photon γ, W^+/W^-, Z^0 and gluon, which are called gauge bosons. In the SM, another boson is the Higgs boson as a quantum excitation of the Higgs field, which is an uncharged and spin-zero scalar boson. The Higgs boson interacts with other particles, causing them to gain mass. For gauge bosons, the Higgs mechanism causes spontaneous symmetry breaking, providing the $W^{\pm}$ and Z bosons to gain mass. In addition, the Higgs boson causes fermions to acquire mass through Yukawa interaction with leptons and quarks. Figure 1.2 provides a pictorial representation of the interactions of all fermions and bosons in the SM.

Photons are the mediator of electromagnetic interaction which is well described by Quantum Electrodynamics (QED) theory. Photons are massless and interact with particles that have an electrical charge. Also, since the photon does not carry its own charge, a photon does not interact with another photon. In addition, the range of the electromagnetic force is infinite due to the zero mass of the photon, but the field strength decreases with an inverse square with increasing distance.

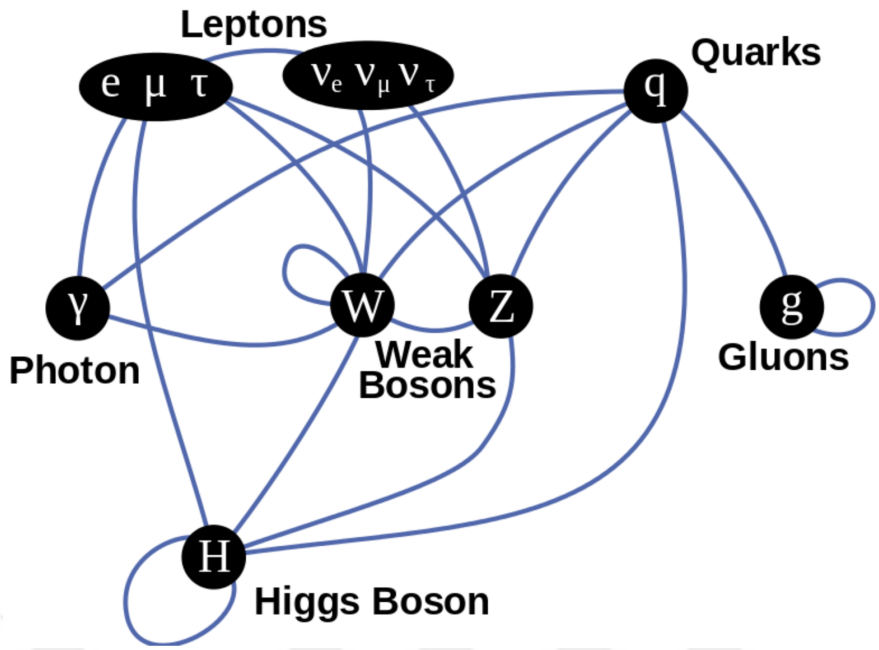

Figure 1.2 : A diagram indicating interactions between fundamental particles in the SM [1].

Electromagnetic and weak interactions can be unified under the $SU(2) \otimes U(1)$ symmetry group as the electroweak theory. In the weak interaction, $W^{\pm}$ and Z bosons play a role in the interactions between particles with different flavors. Due to the parity symmetry-violating nature of the weak interaction, $W^{\pm}$ bosons are only involved in charged-current interactions of left-handed particles and right-handed antiparticles. But neutral charged Z bosons interact with both right-handed and left-handed fermion states. In this sense, fermion fields are stated with chirality components as left-handed doublets and right-handed singlets. The fermions in the SM can be summarized in generations, in table 1.1, with quantum numbers relating to electroweak interaction as weak isospin T, weak hypercharge Y, electric charge $(Q = T_3 + \frac{1}{2}Y)$ which is the conserved quantity. Besides, $W^{\pm}$ bosons can also couple with electromagnetic interaction due to their electrical charge. The coupling constant of the weak interaction is smaller than the coupling constants of the other two interactions which are the electromagnetic and the strong interaction.

Quantum chromodynamics (QCD) as a non-Abelian gauge theory with $SU(3)$ symmetry provides a mathematical description of strong interaction of color charged particles. The mediator particles of the strong interaction are called massless gluons, and gluons have their own color charge, unlike photon in the electromagnetic interaction. There are eight different gluons as a combination of three different colors

Table 1.1 : The SM fermions are illustrated with the associated quantum numbers.

	Generations 1st	2nd	3rd	T	T_3	Y	Q	Color
Leptons	$\begin{pmatrix}\nu_e\\ e^-\end{pmatrix}_L$	$\begin{pmatrix}\nu_\mu\\ \mu^-\end{pmatrix}_L$	$\begin{pmatrix}\nu_\tau\\ \tau^-\end{pmatrix}_L$	$\begin{pmatrix}1/2\\ 1/2\end{pmatrix}$	$\begin{pmatrix}+1/2\\ -1/2\end{pmatrix}$	$\begin{pmatrix}-1\\ -1\end{pmatrix}$	$\begin{pmatrix}0\\ -1\end{pmatrix}$	–
	e_R^-	μ_R^-	τ_R^-	0	0	-2	-1	–
Quarks	$\begin{pmatrix}u\\ d\end{pmatrix}_L$	$\begin{pmatrix}c\\ s\end{pmatrix}_L$	$\begin{pmatrix}t\\ b\end{pmatrix}_L$	$\begin{pmatrix}1/2\\ 1/2\end{pmatrix}$	$\begin{pmatrix}+1/2\\ -1/2\end{pmatrix}$	$\begin{pmatrix}+1/3\\ +1/3\end{pmatrix}$	$\begin{pmatrix}+2/3\\ -1/3\end{pmatrix}$	$\begin{pmatrix}r,g,b\\ r,g,b\end{pmatrix}$
	u_R	c_R	t_R	0	0	+4/3	+2/3	r,g,b
	d_R	s_R	b_R	0	0	-2/3	-1/3	r,g,b

(red, green and blue) and anti-colors, see in table 1.1. The color-carrying property of gluons allows them to interact with each other. In contrast to other forces, the strong force does not decrease as the distance between interacting particles increases. When the distance between two quarks interacting with the strong force reaches a certain limit, the accumulated energy creates a new quark pair (hadron). This phenomenon is called color confinement and therefore free quark cannot be observed.

As mentioned earlier, fermions acquire mass by coupling with a Yukawa interaction term. In order to obtain the mass of the fermions from Yukawa terms, it is important to redefine the fields, moving from flavour states d'_L to mass states d_L, by using unitary matrices $V_{L,R}^{d,u,\ell}$

$$d_{L,R} = V_{L,R}^{d} d'_{L,R}, \quad u_{L,R} = V_{L,R}^{u} u'_{L,R}, \quad \ell_{L,R} = V_{L,R}^{\ell} \ell'_{L,R}. \tag{1.1}$$

Due to the different transformation matrices that transform left-handed up and down type quarks, d, s, and b quarks cannot be described as $SU(2)$ partners of u, c, and t quarks, respectively. To determine the new left-handed doublets in the mass eigenstate basis, the down type components (d'', s'', b'') of the doublets are written as linear combinations of d, s and b quarks:

$$\begin{pmatrix} d'' \\ s'' \\ b'' \end{pmatrix} = \begin{pmatrix} V_{ud} & V_{us} & V_{ub} \\ V_{cd} & V_{cs} & V_{cb} \\ V_{td} & V_{ts} & V_{tb} \end{pmatrix} \begin{pmatrix} d \\ s \\ b \end{pmatrix} \tag{1.2}$$

The unitary transformation matrix called the Cabibbo–Kobayashi–Maskawa (CKM) matrix [6, 7] in the above equation manages the flavour change of the quarks in the $W^{\pm}$ boson interaction. The transition probability from one quark i to another quark j is proportional to the amplitude $|V_{ij}|^2$.

1.1.1 Top quark

The SM successfully explains the characteristics of the leptons and quarks. However, precision measurements of the properties of elementary particles are an important tool for testing known physics and discovering possible anomalies in the SM. In this context, the top quark occupies a special place with its heaviest mass among fundamental particles and its too short lifetime to form a bound state. Its short lifetime provides an opportunity to study the properties of the top quark as a free quark in contrast to the other quarks. Precise measurement of the fundamental parameters associated with the top quark, such as the top quark mass and the three CKM matrix elements including the top, is crucial to a better understanding of the standard model. The relation between top quark mass, W boson mass and the mass of the Higgs boson affects the stability of the Higgs potential. Further, determining the branching ratio of the top quark as accurately as possible is important for new physics search such as the fourth generation.

The top quark decays predominantly into a W boson and a b quark, due to $|V_{tb}|^2$ is almost equal to one. In the decay of the top quark, W boson can occur with different polarizations which are left-handed, right-handed and longitudinal with certain fractions. Deviations in the helicity fractions of the W boson can be an indicator of anomalous Wtb couplings.Consequently, many working groups such as CDF [8], D0 [9], ATLAS [10, 11] and CMS [12] collaborations attempt to pinpoint the top quark intrinsic and decay properties.

This thesis will focus on the properties of the top quark dependent on top quark pair production. In hadron colliders, top quarks are mostly produced as quark pairs under the strong interaction. Unlike weak interactions, which are related to top quarks decay and single top quark production, top quarks are produced in pairs unpolarized due to the parity conservation in QCD [13]. However, since the decay width of the top quarks is much larger than the spin decorrelation scale, the top quarks reflect spin

information through their decay products. Any spin correlation and polarization of top quark in production can be revealed with the angular alignment of decay products. The polarization of the top quark can be determined as follows

$$\frac{1}{\Gamma}\frac{d\Gamma}{d\cos\chi_i} = \frac{1}{2}(1+\alpha_i\cos\chi_i) \tag{1.3}$$

where α_i is the spin analyzing power of the decay product and the χ_i is the angle between the decay product and the spin axis in the top quark rest frame. Besides, the spin correlation of top quarks in pair production is written in general form as

$$\frac{1}{\sigma}\frac{d^2\sigma}{d\cos\chi_i\, d\cos\bar{\chi}_{\bar{i}}} = \frac{1}{4}(1+C_{t\bar{t}}\ \alpha_i\ \alpha_{\bar{i}}\ \cos\chi_i\cos\bar{\chi}_{\bar{i}}) \tag{1.4}$$

here, $C_{t\bar{t}}$ is the spin correlation coefficient, and parameters related to anti-top quark are shown with bar notation. $C_{t\bar{t}}$ varies by different particle colliders such as Tevatron and LHC due to the different initial state dominations and different collision energy. For the LHC, this term is about $+0.311$ at next to leading order (NLO) accuracy while it is equal to -0.389 for the Tevatron [14]. Its value also depends on the choice of the spin basis [14]. In this thesis, the spin correlation and polarization properties of the top quark will be discussed by using 22 observables, explained in detail in ref. [15], associated with the spin correlation of the top-quark pair. The details about the observables can be found in section 3.2.

1.2 Beyond the Standard Model

Although the SM is a theory that has been justified in its predictions and has been verified many times, there are big problems that it cannot explain. Gravity is one of the most important phenomena that the SM cannot explain. Although a hypothetical particle that mediates the gravitational force called the graviton has been added to the SM in order to provide a simple explanation, its existence has not been proven yet. Another unexplained problem is that, unlike the prediction of the SM, the fact that neutrinos have mass has been proven by neutrino oscillation experiments.

The visible universe consists of protons, neutrons and electrons, which are defined as matter and are well explained by the SM. But according to cosmological observations, ordinary matter explains less than 5% of the entire universe. Accordingly, 26% of the universe is filled with a matter called dark matter, which has weak interaction with ordinary matter. And this dark matter cannot be explained by elementary particles in the SM. In addition, the assumed dark energy for the rest of the universe is among the questions that have not yet been resolved. In fact, our theory does not explain that the matter that makes up the visible universe is more than antimatter, which is called the matter-antimatter asymmetry.

Apart from the phenomenological arguments of the problems in the SM, there are also points that cannot be understood theoretically. One of them plays a role in the mass gain of particles by spontaneous symmetry breaking due to the Higgs field. The correction from virtual top quark couplings to the Higgs boson mass is greater than its own mass, that necessitates fine tuning of the bare Higgs mass. This creates a hierarchy problem in the standard model.

These unexplained problems in the SM have pushed physicists to work beyond the standard model (BSM). A large part of BSM studies is comprised of supersymmetry (SUSY). SUSY proposes that each fermion has a boson partner, as a superpartner, and vice versa, see in figure 1.3. The simplest possible supersymmetric model is the Minimal Supersymmetric Standard Model (MSSM), an extension to the SM. MSSM provides solutions to many problems in the SM, such hierarchy problem. In the hierarchy problem, the radiative corrections to the Higgs boson mass become zero by being canceled out with the Yukawa coupling contribution of the superpartners in MSSM. Also in supersymmetry, the lightest superparticle (LSP), in case of R-parity conservation, is a good candidate for dark matter. Because the stable LSP acts as a Weakly interacting massive particle (WIMP), it does not interact with electromagnetic or strong forces.

1.2.1 Top quark in BSM searches

Top quarks are the main background source for most searches of signals beyond the standard model. Large majority of this contribution to background originates from top quark pair production. The top quark pair in a proton-proton collision at a centre

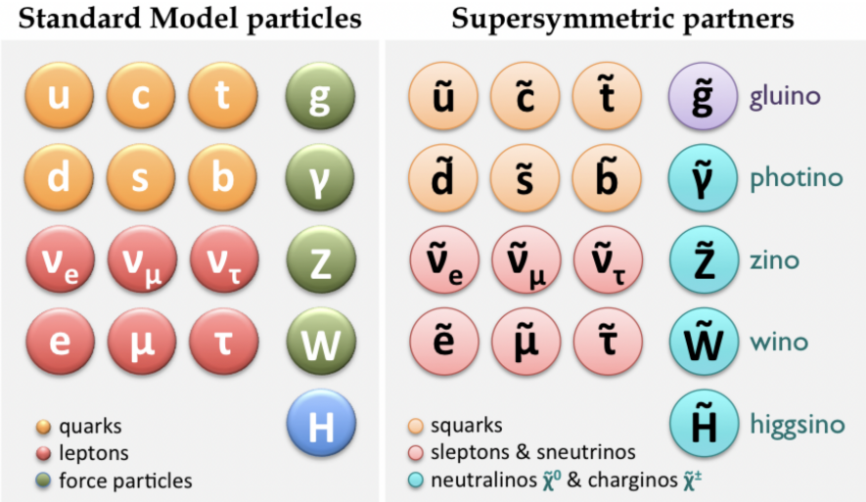

Figure 1.3 : A representation of SM particles and their SUSY superpartners.

of mass energy of $\sqrt{s} = 13$ TeV is produced with the cross section of $831.76^{+19.77}_{-29.20}$ (scale) ± 35.06 (PDF + α_s) pb calculated with the TOP++ (version 2.0) program [16] at next-to-next-to-leading order (NNLO) QCD accuracy, assuming $m_t = 172.5$ GeV. Precision measurement of spin and polarization properties of the top quark pair has a crucial role not only in better understanding the background, but also in the search for new physics.

Searches for bosonic superpartner of top quarks (stop, $\tilde{t}$) and dark matter (DM) candidate particles concentrate generally on high missing transverse energy E_T^{miss} region stem from undetected lightest SUSY particles (LSP), as a decay product of $\tilde{t}$, and DM candidate particles. With these studies, most of the high E_T^{miss} region, even low E_T^{miss}, was excluded by ATLAS and CMS Collaborations [17–20]. In the last step of the study, in section 4.2, we will focus on the interpretation of SUSY and DM signals in low E_T^{miss} region, which are studied with generic searching methods, by measuring precisely. The signals are based on simplified models, which are the similar topology with the models in the ref. [17], of stop pair production and of top quark pair production in associated with fermionic DM candidate particles. In the SUSY signal, in figure 1.4a, a pair of stop $\tilde{t}$ decays an on-shell top quark t and an LSP, in this case neutralino $\tilde{\chi}_1^0$, which is stable for this simplified model. In order to investigate the deviations of the signal from SM $t\bar{t}$, one mass point which is 175 GeV for $\tilde{t}$ and 1 GeV for $\tilde{\chi}_1^0$ will be used.

An alternative dark matter signal in fig. 1.4b include a scalar ϕ or pseudoscalar a spin-0 mediator decayed into fermionic DM particles χ and an associated top quark pair. The coupling strengths of the DM-mediator and the mediator-SM fermions are assumed to be equal to one in the simplified model. Additionally, in this analysis, the scenario with $m_\chi = 1$ GeV and $m_{\phi/a} = 10$ GeV will be focused.

In the above models, we focused on a small mass point to ensure low E_T^{miss}. However, the additional model of R-Parity [21] violating (RPV) SUSY provides more mass points to study for low E_T^{miss} due to the decaying $\tilde{\chi}_1^0$. The $\tilde{\chi}_1^0$ decays into three quarks with the help of a trilinear Yukawa coupling between quarks and superpartner of quarks (squark) [22]. In this study, the production chain includes a $\tilde{t}$ pair decaying into a t and a $\tilde{\chi}_1^0$ as shown in fig. 1.4c, and the $\tilde{\chi}_1^0$ goes into three light flavor quarks, $\tilde{\chi}_1^0 \to uds$, as considered in ref. [23]. For the RPV SUSY scenario, $\tilde{t}$ masses up to 670 GeV have been excluded, by CMS Collaboration [23], at 95% confidence level with a maximum observed local significance of 2.8σ for $m_{\tilde{t}} = 400$ GeV.

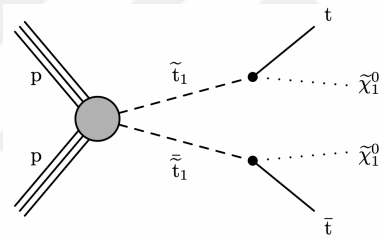

Figure 1.4a : SUSY signal.

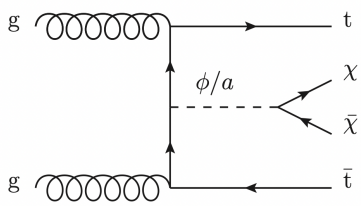

Figure 1.4b : Dark matter signal.

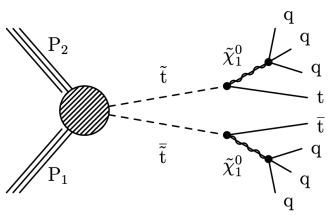

Figure 1.4c : RPV SUSY signal.

Figure 1.4 : Diagrams of the signal samples.

1.3 The Large Hadron Collider Experiment

Accelerators were invented in the 1930s to study the structure of the atomic nucleus with high-energy particles. Later, they diversified and started to serve different purposes. In principle, accelerators give kinetic energy to the particle beams with the electric field, while at the same time directing and focusing them with the magnetic field. Accelerators are separated from each other according to the purpose of the experiment. As the largest and most powerful in the world, the Large Hadron Collider (LHC) is involved in accelerating protons and heavy lead ions and colliding them at high energies. The LHC is a circular accelerator with a total length of 27 kilometers. It is designed so that the center of mass energy of two colliding protons reaches $\sqrt{s} = 14$ TeV. Since the LHC began operating in March 2010, the energies of the colliding proton beams have been gradually increased, now the energy of each proton beam is 6.5 TeV. There are 8 detectors for collision experiments on the LHC, four of which are the major detectors A Large Ion Collider Experiment (ALICE), A Toroidal LHC Apparatus (ATLAS), the Compact Muon Solenoid (CMS), and the Large Hadron Collider beauty (LHCb). ATLAS and CMS are general purpose particle detectors, while ALICE and LHCb have more specialized functionality.

The CMS detector will be discussed since data from CMS Collaboration are used in this thesis. CMS is a general purpose particle physics detector just like ATLAS and these two detectors are designed for similar purposes. Having the same purpose but differences in design is important for these two detectors to complement each other and confirm the findings. The CMS detector is made up of layers, each layer has a different task which are measurement of the trajectories of charged particles (silicon tracker), determination of the energies of electrons and photons with high accuracy (electromagnetic calorimeter (ECAL)), measurement of energies of hadrons (hadron calorimeter (HCAL)), providing strong magnetic field of 3.8 T (the magnet) and detecting muons.

2. MONTE CARLO EVENT GENERATORS IN PARTICLE PHYSICS

Monte Carlo (MC) event generators are essential tools in high energy physics (HEP) to simulate the processes at collider experiments. Many experimentalists and theorists make use of MC to make predictions for collider experiments and to design analysis strategies. MC event generators have several steps to describe the final states of high energy particle collisions which are starting from short distance scales to the scale of hadronization and decay. In this chapter the philosophy of simulation of collisions and steps in production of events will be explained.

2.1 Theoretical Foundation of Event Generation

The interactions of subatomic particles under quantum effects are not deterministic, unlike classical physics. The transition of a particle from one quantum state to another can only be calculated as probability. The transition rate $P_{i\to f}$ of a quantum system is defined, in a general form, by Fermi's golden rule as follows

$$P_{i\to f} = \frac{2\pi}{\hbar}|M|^2\rho \tag{2.1}$$

where ρ is the density of final states, the so-called phase space factor, and it holds kinematical information of the transition of the quantum states. The probability of transition from the state $|i\rangle$ to the state $|f\rangle$ is proportional to the matrix element M, which can be written as $\langle f|V_I|i\rangle$ in explicit form, for interaction potential V_I. The matrix element includes dynamical information about the transition, Feynman diagrams provide convenience in its calculations. Fermi's golden rule can calculate the decay rate of a particle, as well as cross section of a scattering process from two particles to multiple particles. With the help of the equation (2.1), the differential cross section $d\sigma$ of a scattering $1+2\to 1^{'}+2^{'}+...+n^{'}$ is given by

$$d\sigma = \frac{1}{u_\alpha}\frac{1}{2E_1}\frac{1}{2E_2}\overline{|M|^2}(2\pi)^4\delta^4(p_1+p_1-p_1^{'}-...-p_n^{'})\prod_{i=1}^{n}\frac{d^3p_i^{'}}{(2\pi)^3 2E_i^{'}} \tag{2.2}$$

where $\overline{|M|^2}$ is the matrix element averaged over particle spins and u_α is the relative velocity of two initial particles

$$u_\alpha = \frac{\sqrt{(p_1.p_2)^2 - m_1^2 m_2^2}}{E_1 E_2} \tag{2.3}$$

As mentioned earlier, the matrix element comprises dynamical information of the scattering process and allows us to calculate the amplitudes of the scattering processes with Feynman diagrams. Feynman diagrams are pictorial representations that model mathematical descriptions of particle interactions. As seen in figure 2.1, the scattering process $(e^+e^- \to \mu^+\mu^-)$, which is an instructive process for the diagram concept, is presented by a Feynman diagram. The diagram is shown in $1+1$ space-time dimension, and time flows from left to right for this representation. The external lines represent incoming and outgoing particles with having momentum $\mathbf{p}_i$ and spin σ_i. The inner line is also called propagator of interaction. In addition, each point where the lines meet in the diagram is defined as vertex.

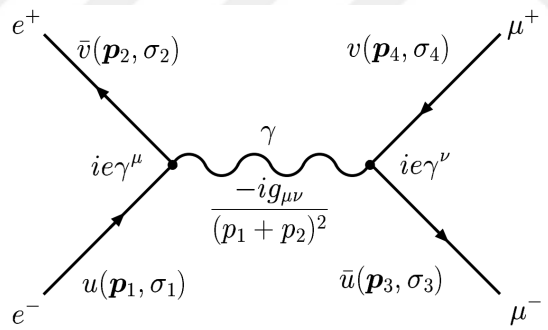

Figure 2.1 : A tree-level Feynman diagram of the $(e^+e^- \to \mu^+\mu^-)$ scattering process [2].

The amplitude M of the scattering process is calculated by Feynman rules which are exhibited as pictorially in figure 2.1 [24]

$$-iM = [\bar{u}(\mathbf{p}_3, \sigma_3)(ie\gamma^\nu)v(\mathbf{p}_4, \sigma_4)]\frac{-ig_{\mu\nu}}{(p_1+p_2)^2}[\bar{v}(\mathbf{p}_2, \sigma_2)(ie\gamma^\mu)u(\mathbf{p}_1, \sigma_1)] \tag{2.4}$$

The Feynman diagram given in figure 2.1 is the tree level diagram for $(e^+e^- \to \mu^+\mu^-)$ scattering process, that is, the diagram has the highest contribution to perturbative

expansion of the S-Matrix [2]. In the calculation of cross-section, the lowest order term in perturbation theory that has the highest contribution is called leading order (LO). The LO calculations comprise only leading order Feynman diagrams. For example, the leading-order Feynman diagrams for $pp \to t\bar{t}$ are shown in figure 2.2. On the other hand, it can be acquired more accurate results by calculating higher-order terms. Today, the next-to-leading order (NLO) calculations have been successfully integrated into MC event generators. The Feynman diagrams at NLO accuracy involve one-loop diagrams, initial-state radiation (ISR) [25] and final-state radiation (FSR) [26] contributions. Another advantage of the NLO for LO is that it reduces the scale dependency. But it needs more computation time for the same process compared to LO.

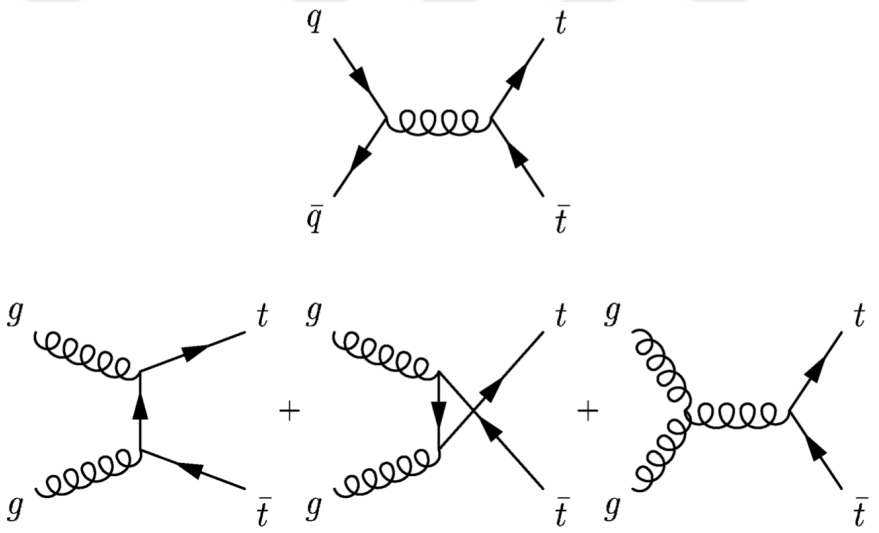

Figure 2.2 : The lowest order Feynman diagrams for top quark pair production [3].

The above-mentioned cross-section calculations contain a large amount of QCD contributions. But with high energies, the observables become more sensitive to electroweak (EW) contributions, which is suppressed due to having a small value of coupling constant α, by large Sudakov logarithms originating from the virtual exchange of soft and collinear weak bosons [27, 28]. Therefore, electroweak contributions are becoming more important for MC calculations.

The partons (such as quarks and gluons) used in the cross-section calculations by making use of perturbative QCD are not observed in free form in real collider experiments due to color confinement [29, 30]. The hadrons which are the initial

states of scattering processes in collision experiments give problem in the calculation of cross-section due to their composite structures. For these reasons, the calculation of the total cross-section or other quantities for the scattering process is divided into two parts, by using factorization theorem, as hard and soft [31, 32]. For the hard process in high energy, short-distance interactions are predicted by using perturbative QCD. Contrarily, the cross section calculation in the soft process is no longer in the perturbative region. Hence, the effect of the soft process coming from long-distance interactions can be determined by experimental models. With the above definitions, the total cross section for colliding hadrons is described as

$$\sigma_{AB\to ab} = \sum_{i,j} \int_0^1 \int_0^1 dx_1\, dx_2 \phi_{i,A}(x_1,\mu_F)\phi_{j,B}(x_2,\mu_F)\hat{\sigma}_{ij\to ab}(Q^2,\mu_F) \tag{2.5}$$

where the functions $\phi_{i,A}$ and $\phi_{j,B}$ which is called as parton distribution functions (PDF) define the probability of finding parton $i(j)$ with longitudinal momentum fraction $x_1(x_2)$ in related hadron $A(B)$ by setting factorization scale μ_F to a certain value. Parton distribution functions continue to be developed by various groups such as CTEQ [33] Collaboration, Martin Motylinski Harland-Lang Thorne (MMHT) [34] Collaboration and NNPDF [35] Collaboration using different experimental data in the non-perturbative region, as mentioned earlier. The partonic cross section $\hat{\sigma}_{ij\to ab}(Q^2,\mu_F)$ holds the parton level hard scattering, with the virtuality Q^2 and the factorization scale μ_F which determine whether it belongs to the hard process or parton distribution function.

2.2 Steps in the Generation of the Events

The basic aim of Monte Carlo event generators is to simulate the high amount of scattering processes with approximations based on quantum field theory. Event generation is done by dividing into several steps due to the factorization theorem mentioned in the previous section. A hadron collider event is presented with seperate components corresponding to different kinematic regimes in figure 2.3. According to this pictorial representation, the hard process, in this case $t\bar{t}h$ production, is illustrated by big red disc with parton-level final states (three small red discs). Additional QCD radiations, before and after parton-level final states, modeled by the parton shower are

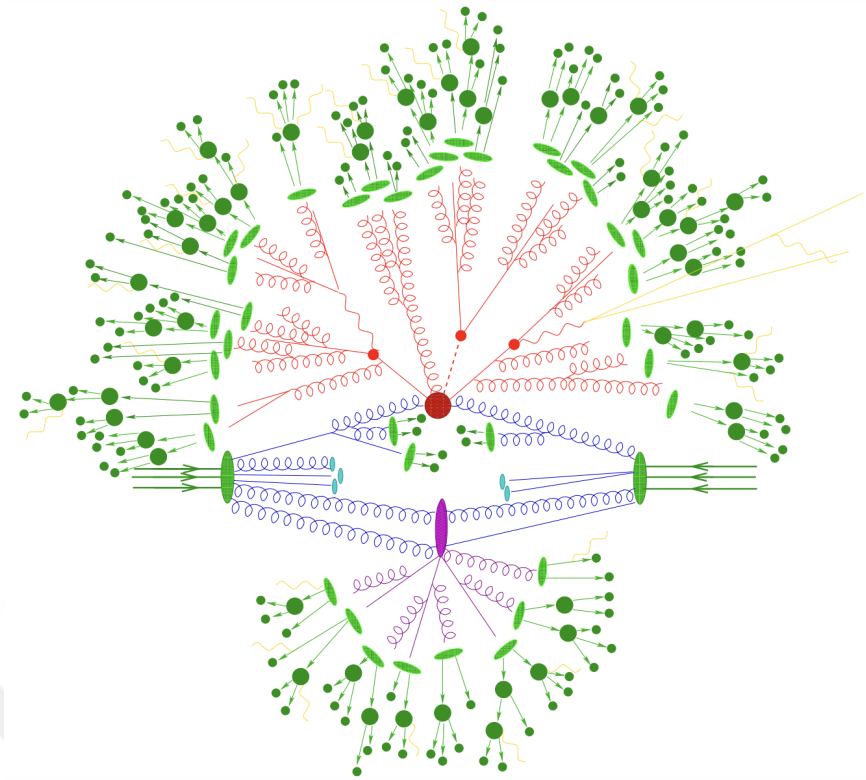

Figure 2.3 : The structure of a $t\bar{t}h$ event generated by an event generator. All separate steps are represented by different colors: the hard process in red, hadronization in light green, hadron decay in dark green, underlying events in purple and photon radiation in yellow [4].

shown as red helices and lines. Partons with momentum low enough for hadronization occur as hadron-bound states (light green discs) by considering phenomenological fragmentation models. As the last step of the production, colorless hadrons are decayed into particles which some can be detected in experiments (dark green discs). Besides, it can be seen, with yellow lines, radiation of photons at any stage. Collisions, apart from the main process, resulting from remnants of protons are called underlying events and are shown in purple in figure 2.3. To simulate collider events, various Monte Carlo event generators follow the steps mentioned above with different approaches using different tools. In the following subsections, more details will be given about each step and the methods used by MC generators during these steps.

2.2.1 Hard process

As the first step in event generation, the hard process, which is the heart of the scattering, is employed. The hard process gives the probability of scattering with the initial-state as incoming partons with high momentum described by parton distribution

functions (PDF) by applying the matrix element method. The small strong coupling constant α_s allows perturbation theory to be used for this process. However, the order in QCD perturbation theory is vital for accuracy in calculation. It affects the precision of all probability distributions of events. Matrix element (ME) event generators handle the hard process with leading order (LO) or next-to-leading order (NLO) accuracy. Next-to-next-to-leading (NNLO) is not yet integrated into event generators, but this is expected in the near future.

As discussed above, MC event generators consist of modular structure, just as in cross-section calculation using factorization theory. ME generators are also part of it. MC event generators are generally divided into two: the general purpose Monte Carlo (GPMC) generators and the generators where the hard process and parton shower are performed in separate structures. To introduce briefly, GPMC generators simulate all high energy physics processes, more information can be found in [36]. The other type of MC event generator is called ME+PS or NLO+PS according to the order of perturbation theory calculated by the matrix element module.

Two GPMC generators used in this thesis will be mentioned. Beginning with PYTHIA8, it is one of the most frequently used event generator [37]. PYTHIA8 contains a wide range of $2 \to n$ hard subprocesses, but it will be used in this study as a parton shower module for ME+PS and NLO+PS. SHERPA is the other GPMC event generator that will be discussed. It is quite new amongst the other MC generators. SHERPA having two matrix-element generators as AMEGIC++ and COMIX provides LO and NLO calculations in QCD for a large spectrum of subprocesses. Based on Feynman diagrams, AMEGIC++ converts them to helicity amplitudes and performs matrix element calculations. For the highest multiplicity processes, COMIX is a convenient module. COMIX employs the Berends-Giele recursive relation to deal with color in tree-level matrix elements [38, 39]. This gives an advantage to COMIX in performance for large final state multiplicities against AMEGIC++ [36]. In addition, OPENLOOPS, which is an generator of one-loop amplitudes, is utilized within SHERPA for evaluation of virtual corrections at NLO accuracy. OPENLOOPS algorithm combined with on-the-fly reduction methods is carried out in computation of loop integrals.

The method of Matrix Element and Parton Shower (ME+PS) or NLO and Parton Shower (NLO+PS) matching is frequently used in simulation of high energy physics

processes. This type of calculations rely on different MC event generators for matrix element and parton shower steps. MADGRAPH5_AMC@NLO is a unified framework including MADGRAPH5 which operates LO and AMC@NLO which operates NLO calculations. MADGRAPH5 uses helicity amplitude method in evaluating the squared matrix element of the processes, with ALOHA module. For determining the virtual contributions at NLO accuracy, MADGRAPH5_AMC@NLO employs a module named MADLOOP. With this module, Ossola-Papadopoulos-Pittau (OPP) and Tensor Integral Reduction (TIR) techniques are applied as reduction methods for one-loop integrals. The former one of these techniques is the main procedure in MADLOOP. The last matrix element event generator that will be discussed for this thesis is POWHEG BOX. It implements a method that uses NLO QCD real emission matrix element to generate the hardest emission. Additionally, the POWHEG BOX cannot be used for an arbitrary process due to it is organized as packages for each specific process. It is difficult to say that POWHEG BOX uses a particular method to generate events. However, for this thesis, POWHEG BOX will only be used for top quark pair production. In this package, the MCFM [40–42] matrix elements with the narrow width approximation have been implemented for hard process by authors [43]. As an advantage to MADGRAPH5_AMC@NLO, the NLO computations in the POWHEG BOX are independent of the parton shower after matrix element.

2.2.2 Parton shower

The parton shower deal with the evolution of the initial- and final-state partons in the hard process. Quarks and gluons as partons are coloured particles and can emit QCD radiation as gluons. In Quantum Electrodynamics (QED), Bremsstrahlung is a well-known phenomenon in which scattered electrically charged particles radiate photons. As in QED, colour charged particles radiate gluons in each step of collision (ISR and FSR). However, gluons have a colour charge different from photons so they can interact with each other by gluon radiation. This induces parton shower, and soft and collinear partons continue to radiate until the hadronization. Generally, the parton shower procedure relies on collinear parton splitting and soft gluon emission. This leads to filling up phase space at higher orders in perturbation theory, that matrix element cannot reach.

There are different kinds of event generators to implement parton shower, two of them are covered by this thesis. PYTHIA8 mentioned in the previous subsection uses transverse momentum ordered parton shower method which is based on an evolution in energies starting with highest p_T up to a cutting energy [44]. The second event generator for parton shower is Sherpa which contains two different parton showers having different perspectives to fill the phase space in perturbation theory for multiple radiations of subsequent particles. CSSHOWER, which is the default one, based on Catani-Seymour factorisation terms [45, 46]. According to the CSSHOWER, soft gluons are modelled as dipole which holds a splitting parton and a colour connected parton, and these dipoles continue to splitting throughout the shower [47]. The other parton shower module in SHERPA is DIRE [48]. It is based on Catani-Seymour factorisation as in CSSHOWER, but they differ in parton evolution. In this thesis, the CSSHOWER module will be considered in the SHERPA parton shower.

2.2.3 Matching and merging

The matrix element and the parton shower are complementary procedures for phase space of perturbation theory in describing a scattering event. Matrix element event generators define high-energy and separated partons in hard process very well. Calculating more additional hard partons is important for the correct description of the process. However, it adds an extra burden in the computation of matrix element. To address this issue, parton shower event generators are used due to having no restriction on particle multiplicity. It is important to use both technics in order to get the best definition of data. In combination of matrix element and parton shower, some procedures are implemented to avoid double counting of additional jets and to ensure a smooth transition in phase space. The double-counting problem can be explained as the Feynman diagram with more than zero extra partons produced by the matrix element is the same as produced by the parton shower with the same number of extra partons. To deal with it, many technics are available for merging matrix element and parton shower. In merging matrix element and parton shower, MLM, FXFX and CKKW are common techniques by dividing the phase space with a merging cut for additional jets. Matching NLO matrix element and parton shower is more complicated process compared to LO, thus MC@NLO and POWHEG methods are used to deal with this challenge.

2.2.4 Fragmentation and hadronization

Hadronization is long distance process in which low energy partons that emitted gluon and splitted, form hadrons due to the color confinement. After the parton shower, the hadronization process occurs with partons having enough low energy for non-perturbative region and it creates hadrons which is colorless bound states. Most of the hadrons have small lifetime and decay into other particles which can be observed in a short time. To describe the hadronization process, several methods are currently used in event generators and mostly these methods have experimental parameters due to non-perturbative interactions. Two commonly used methods as cluster [49] and Lund string model [50] will be mentioned. The cluster model is based on color neutral clusters formed by quarks and gluons from parton shower. According to this approach in figure 2.4, final state gluons split into quark-antiquark pairs then these color connected pairs form color neutral clusters. After the clustration, the resonance states decay into smaller clusters and hadrons. In the Lund string model, the color flux between quark and antiquark is represented as a string as seen in figure 2.4. If energy density in the color field is high enough, the strings break into quark-antiquark pairs. The string model require additional parameters compared to former model for the transverse momentum distribution, and damping of heavy particles [5].

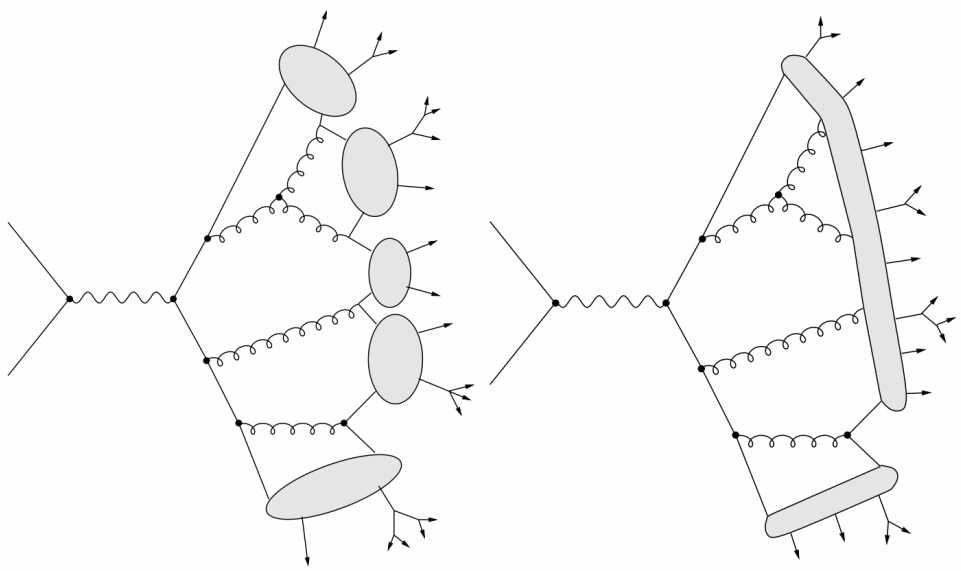

Figure 2.4 : Schematic representation of the cluster (left) and the string (right) models [5].

2.2.5 Underlying events

The rest of the hadron-hadron collision apart from the hard process is called beam remnant. Due to the composite structure of hadrons, each collision leaves behind a beam remnant. Beam remnants include pairs of partons that split and radiate gluons, so-called multiple interactions, and this contributes to the hadronization step with emitted partons. Thus, these underlying events are considered in Monte Carlo event generators by using some approximations.

2.3 Fast Detector Simulation

A wide range of final states is created in high energy particle collisions as discussed in previous sections. In experiments, huge detectors as ATLAS and CMS are used to detect particles obtained from such collisions. On the theoretical prediction side, detector simulations are employed to perform detector response with a specific topology by concerning the output of Monte Carlo event generators. Fast detector simulations like DELPHES [51] are used in most phenomenological studies while there are highly detailed and accurate detector simulations. Such simulations are computationally much faster than full detector simulations and this is the reason for the high usage of fast detector simulations. In this thesis, DELPHES will only be used to work in the "root" file format, all events will be considered at the generator level.

3. SPIN CORRELATION AND POLARIZATION FOR TOP QUARK PAIRS AT THE LHC

In this chapter, a technical foundation of the study will be established. Firstly, it will be given a general picture of the analysis. Next, the MC data samples used in the analysis will be explained in detail. MC event generator settings for all $t\bar{t}$ and signal samples will be presented. The chapter will be concluded with the description of the set of observables of spin correlation and polarization in top quark pair production by using decomposition of spin density matrix.

3.1 Analysis and Computational Setup

3.1.1 Analysis flow

As mentioned in the previous chapter, Monte Carlo (MC) event generators are significant tools in data analysis for high energy physics and in QCD modelling. They are used often to predict behaviours of physical objects in collision processes. In this sudy, three different MC event generators which are MADGRAPH5_aMC@NLO, SHERPA and POWHEG BOX, were used to simulate the high energy physics events.

A flow chart which summarizes the analysis procedure is given in figure 3.1. According to the scheme, the first step covers the hard process of a collision event. Afterward one is applied to the samples parton shower to evolve the events more. But it is important to note that SHERPA as a general purpuse MC event generator performs both the first and the second steps. For events generated by ME event generators MADGRAPH5_aMC@NLO and POWHEG BOX, PYTHIA8 was used to implement the parton shower. The parameter cards for all samples used in the study can be found in Appendix A. After the full simulation of the collision events including hadronization, decay and underlying events, the DELPHES detector simulation is implemented on the samples to make them suitable for comparison with data. On the other hand, in the detector simulation, the generator level particle information will be used. With this procedure, each particle kinematic information in the events can be used without

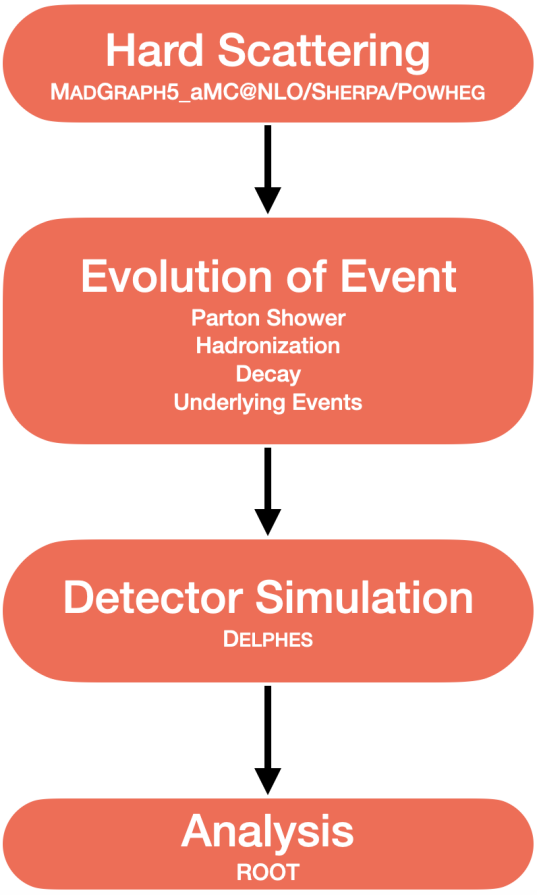

Figure 3.1 : A representative flowchart of the analysis.

needing of reconstruction. As a last step, the generator level particle information taken from DELPHES output is employed, with the ROOT [52] data analysis framework, in the calculation of observables which will be detailed in the next sections.

3.1.2 Monte Carlo data samples

A range of MC generators to provide predictions for top quark pair production and related BSM signal processes are used to investigate the effects of various approaches of MC generators on top pair spin correlation matrix and polarization variables and to assess the differences between BSM signals and top quark pairs.

A summary of the produced MC samples, describing various the SM top quark pair production processes and the possible signal scenarios, is shown in table 3.1. The table also lists details of the simulation samples used, including the matrix element (ME) event generator with the order of the calculation and the central parton distribution function (PDF) set, the parton shower (PS) and hadronization model, and the merging scheme used to remove the overlap between ME and PS.

Table 3.1 : Matrix Element (ME) event generator settings for $t\bar{t}$ and BSM signal samples used in this study. The generator versions, the order of QCD accuracy of associated predictions, the PDF sets used in ME calculations and the merging scheme are shown.

Process	Order	ME event generator	ME PDF	PS and hadronization	Merging scheme
$t\bar{t}+jets$	NLO	MG5_aMC@NLO 2.6.7	NNPDF3.0NLO	PYTHIA 8.2.44	FxFx
$t\bar{t}+jets$	LO	MG5_aMC@NLO 2.6.7	NNPDF3.0LO	PYTHIA 8.2.44	MLM
$t\bar{t}+jets$	NLO	POWHEG BOX (v2)	NNPDF3.0NLO	PYTHIA 8.2.40	POWHEG ($h_{damp} = 272.72$ GeV)
$t\bar{t}+jets$	NLO (EW)	SHERPA 2.2.8	NNPDF3.0NLO	CSSHOWER	MEPS@NLO
$t\bar{t}+jets$	LO	SHERPA 2.2.8	NNPDF3.0LO	CSSHOWER	MEPS
$\tilde{t}\tilde{t} \to t\tilde{\chi}_1^0\bar{t}\tilde{\chi}_1^0$	LO	MG5_aMC@NLO 2.4.2	NNPDF3.1LO	PYTHIA 8.2.40	MLM
$t\bar{t}+DM$	LO	MG5_aMC@NLO 2.6.1	NNPDF3.1LO	PYTHIA 8.2.40	MLM

All signal and $t\bar{t}$ samples are processed using DELPHES (3.4.2) [53] to provide the simulation of CMS detector due to the real data comparison. In all $t\bar{t}$ and signal samples, $t\bar{t}$ events are produced with a top quark mass of $m_t = 172.5$ GeV. The nominal $t\bar{t}$ sample (with up to two additional matched partons included in the ME calculations) is simulated using MADGRAPH5_aMC@NLO (v2.6.7) [54] at NLO QCD accuracy. To evaluate the effects of different perturbative orders of the calculation, we have been used the samples generated with MADGRAPH5_aMC@NLO at LO accuracy as well. The parton showers are modelled using PYTHIA (v8.2.44) [44] with the default showering tunes. The matrix elements at LO and NLO are merged with the parton shower using the MLM [55] and the FxFx [56] merging scheme, respectively. In order to determine state-of-the-art theoretical approaches between the different methods in MC generators, two additional generator setups are incorporated in the analysis chain. Firstly, $t\bar{t}$ sample is generated using the SHERPA (v2.2.8) [47] generator with up to two and three extra partons at LO and NLO, respectively. The SHERPA, in production of $t\bar{t}$ events, employs COMIX [57] and OPENLOOPS [58–60] in matrix elements calculation which are merged with CSSHOWER [46] for parton showering and hadronization by using the MEPS@NLO [61,62] prescription. To match the ME and PS results, SHERPA and MADGRAPH5_aMC@NLO make use of the same normalization method, which is MC@NLO [63]. The other alternative $t\bar{t}$ sample is generated with POWHEG BOX (v2) [64–67] including up to two extra matched partons at the ME level with NLO accuracy. The parton shower is employed by PYTHIA (v8.2.40) with $h_{damp} = 272.72$ GeV parameter of POWHEG.

For all SM samples listed, the initial state partons are modeled with the NNPDF3.0 PDF set [35, 68] implemented by LHAPDF [69]. To determine the systematic uncertainties in predictions, uncertainties coming from PDF and scale variations are used as summed in quadrature. Parton distribution function uncertainties are evaluated by reweighting the $t\bar{t}$ samples generated by MADGRAPH5_aMC@NLO at LO and SHERPA for all setups using generator weights related with each of the variations given by NNPDF3.0, CT10 [33] and MMHT14 [34] PDF sets. Renormalization and factorization scale uncertainties are calculated using variations by a factor of two around the central scales which are equal to $\frac{1}{2}\sum_{i=1}^{2}\sqrt{m_t^2 + P_{T,i}^2}$ for

MADGRAPH5_aMC@NLO and $m_t^2 + \frac{1}{2}\sum_{i=1}^{2} P_{T,i}^2$ for SHERPA setup [70], where $P_{T,i}$ is the transverse momentum of top quarks.

Signal samples of SUSY and RPV SUSY are simulated at LO with up to three and two additional partons, respectively, with MADGRAPH5_aMC@NLO (v2.4.2) interfaced to PYTHIA (v8.2.40) for parton showering and hadronization using the MLM merging scheme. For the SUSY sample in fig. 1.4a, the masses of the $\tilde{t}$ and the $\tilde{\chi}_1^0$ will be considered as $m_{\tilde{t}} = 175$ GeV and $m_{\tilde{\chi}_1^0} = 1$ GeV. On the RPV SUSY side, the masses of the $\tilde{t}$ and the $\tilde{\chi}_1^0$ are taken as 400 GeV and 100 GeV, respectively.

The other signal samples are top quark pairs associated with DM particles χ as shown in fig. 1.4b which is included scalar ϕ or pseudoscalar a mediators. The DM signal samples are simulated at LO including up to one additional parton with MADGRAPH5_aMC@NLO (v2.6.1) interfaced with the PYTHIA (v8.2.40) PS model using the MLM merging scheme. The masses of the χ and the ϕ/a will be considered as $m_\chi = 1$ GeV and $m_{\phi/a} = 10$ GeV. In all signal samples, NNPDF3.1 PDF set is used in ME calculation.

To assess the truth of the theoretical predictions, experimental measurements published by CMS Collaboration are directly used [71]. The CMS analysis unfolded the data to compare with parton level predictions at full phase space. In our analysis, the MC predictions have baseline selections compatible with the CMS analysis.

3.2 The Formalism of the Spin Density Matrix

The total cross section for the top pair production at accelerator energy s can be written as

$$\sigma(s, m_t) = \sum_{i,j} \int_0^1 \int_0^1 dx_1\, dx_2 \phi_{i,A}(x_1, \mu_F)\phi_{j,B}(x_2, \mu_F)\hat{\sigma}_{ij\to t\bar{t}}(\frac{m_t^2}{\hat{s}}, \mu_R, \mu_F, \alpha_s(\mu_R)) \tag{3.1}$$

by using factorization theorem. This theorem divides the total cross section into a short distance (hard) part $\hat{\sigma}_{t\bar{t}}$ and a long distance (soft) part, which is known as parton distribution function $\phi_{i,A/j,B}$ (PDF). The PDF determine the probability of the existence of a parton i (j) in the hadron A (B) with a rate x_1 (x_2) of the longitudinal momentum of the hadron at the factorization scale μ_F. The partonic cross section $\hat{\sigma}_{ij\to t\bar{t}}$ involves

the spin information of top quark and anti-quark. However the spin information of a top quark is not detectable because of short life time of it. In spite of the fact that the spin of an unstable particle produced in high energy reactions is no straightforwardly noticeable quantity, it is extremely helpful to present the idea of a spin density matrix [72] for the top pair system (3.2). The decay width of the top quark much smaller than its mass allows to use narrow width approximation (NWA) [73, 74]. Using NWA, the matrix element of the top pair production can be written as the trace of the production and the decay factors:

$$|M|^2 \propto Tr[\rho R \bar{\rho}] \tag{3.2}$$

where R is the spin density matrix of the on-shell top pair production and ρ and $\bar{\rho}$ are the decay spin density matrices of the polarized top quark and antiquark, respectively. To look at the spin properties of the top quark and antiquark, spin density matrix can be decomposed in the spin space of t and $\bar{t}$.

$$R \propto \tilde{A} I \otimes I + \tilde{B}_i^+ \sigma^i \otimes I + \tilde{B}_i^- I \otimes \sigma^i + \tilde{C}_{ij} \sigma^i \otimes \sigma^j \tag{3.3}$$

Here, the first terms which are a 2x2 unit matrix (I) and the Pauli matrices σ^i in the tensor products refer to top spin spaces, and second terms refer to anti-top.

While the function $\tilde{A}$ is related to the total $t\bar{t}$ cross section and the top quarks kinematic properties, $\tilde{B}_i^{\pm}$ and $\tilde{C}_{ij}$ are 3-vectors that describe the polarizations of t and $\bar{t}$ in each direction, and 3x3 matrix that determine the spin correlation between top quark and antiquark.

As mentioned earlier, decay of the top quarks before hadronization allows to study the spins of them by looking at the angular distribution of the decay products. Top quarks decay almost to a W boson and a bottom quark. The final states of the decay coming from W boson can be a quark-antiquark pair or a lepton and a neutrino. The angular

distribution of the top decay products with respect to the spin alignment of the top is given by

$$\frac{1}{\Gamma}\frac{d\Gamma}{d\cos\chi_i} = \frac{1}{2}(1+\alpha_i\cos\chi_i) \tag{3.4}$$

with χ_i the angle between the 3-momentum of decay product i in the top rest frame and the direction of the top spin. α_i is the spin analyzing power of i. The spin analyzing power of the charged lepton is almost equal to 1 which is maximum value. For a top antiquark, α_i is minus sign of the top quark one. It does not change much at NLO QCD [75]. To make use of high valued spin analyzing power, leptons have been used as a proxy for spins of top quarks and anti-quarks.

The functions $\tilde{B}_i^{\pm}$ and $\tilde{C}_{ij}$ in equation (3.3) can be written as a linear combination of coefficient functions associated with an orthonormal basis. The basis in this analysis was chosen as the helicity basis as it gives more spin correlation compared to other alternatives as discussed in ref. [14]. This basis can be shown in figure 3.2. $\hat{k}$ is described as helicity axis determined by the top quark direction in the $t\bar{t}$ center-of-mass (CM) frame. The direction $\hat{p}$ indicates the direction of one of the incoming parton in the same frame. Using the directions $\hat{k}$ and $\hat{p}$, the normal $\hat{n}$ to the scattering plane and the direction $\hat{r}$ perpendicular to $\hat{k}$ in the scattering plane are given by $\hat{n} = (\hat{p}\times\hat{k})/\sin(\Theta)$ and $\hat{r} = (\hat{p}-\hat{k}\cos(\Theta))/\sin(\Theta)$.

A redefinition of the $\hat{r}$ and $\hat{n}$ axes is necessitated owing to the Bose-Einstein symmetry of the initial gg state [15]. The reference axes $\hat{a}$ and $\hat{b}$ are described with above regularization as

$$\hat{a} \to \{\hat{k}, sign(\cos\Theta)\hat{r}, sign(\cos\Theta)\hat{n}\},\ \hat{b} \to \{-\hat{k}, -sign(\cos\Theta)\hat{r}, -sign(\cos\Theta)\hat{n}\} \tag{3.5}$$

Using the orthonormal basis, $\tilde{B}_i^{\pm}$ and $\tilde{C}_{ij}$ are decomposed as

$$\tilde{B}_i^{\pm} = b_k^{\pm}\hat{k}_i + b_r^{\pm}\hat{r}_i + b_n^{\pm}\hat{n}_i, \tag{3.6}$$

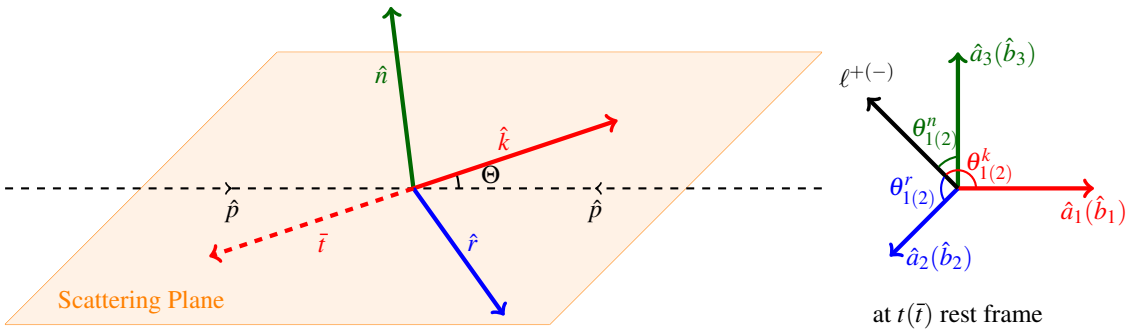

Figure 3.2 : Coordinate system illustrating t and $\bar{t}$ helicity spin basis. The $\hat{k}$ axis is described as the direction of flight of top quark measured in the $t\bar{t}$ CM. The directions $\hat{k}$, $\hat{r}$, $\hat{p}$ and $\bar{t}$ are in the scattering plane which the normal is the direction $\hat{n}$. The signs of the $\hat{r}$ and $\hat{n}$ axes can have inverse according to the angle Θ as shown in equation (3.5). The angles between the direction of flight of the positively ℓ^+ (negatively ℓ^-) charged lepton in the top quark (anti-quark) rest frame and the axes $\hat{a}$ ($\hat{b}$) determined in equation (3.5) are used to calculate the coefficients in equations (3.9)-(3.12).

$$\begin{aligned}\tilde{C}_{ij} &= c_{kk}\hat{k}_i\hat{k}_j + c_{rr}\hat{r}_i\hat{r}_j + c_{nn}\hat{n}_i\hat{n}_j \\ &+ c_{rk}(\hat{r}_i\hat{k}_j + \hat{k}_i\hat{r}_j) + c_{nr}(\hat{n}_i\hat{r}_j + \hat{r}_i\hat{n}_j) + c_{kn}(\hat{k}_i\hat{n}_j + \hat{n}_i\hat{k}_j) \\ &+ c_n(\hat{r}_i\hat{k}_j - \hat{k}_i\hat{r}_j) + c_k(\hat{n}_i\hat{r}_j - \hat{r}_i\hat{n}_j) + c_r(\hat{k}_i\hat{n}_j - \hat{n}_i\hat{k}_j)\end{aligned} \tag{3.7}$$

The coefficient functions $b_i^{\pm}$, c_{ij} and c_i which are functions of the partonic center of mass-energy $\hat{s}$ and $\cos\Theta$ are related to some discrete symmetries such as parity (P) and charge-parity (CP), and they are summarized in table 3.2.

According to table 3.2, the P- and CP-even coefficient functions (c_{kk}, c_{rr}, c_{nn} and c_{rk}) can have large values due to the parity invariance of strong interaction. However, the presence of electroweak (EW) corrections can result in non-zero P-odd and CP-even coefficients (c_{nr} and c_{kn}). On the other hand, the coefficients produced by CP-violating interactions are close to zero in the SM. The approximate CP invariance of the SM limits the top and anti-top quarks to have the same polarization, so $b_i^+ - b_i^-$ has a value of zero.

After the equations (3.2) and (3.3), the normalized distribution for the two leptons final state can be written in the form of spin coefficients and direction of flight of the leptons.

Table 3.2 : Observable quantities of the spin density matrix and their corresponding measured coefficients, coefficient functions and P and CP symmetry properties.

Observable	Measured coefficient	Coefficient function	Symmetries
$\cos\theta_1^k$	B_1^k	b_k^+	P-odd, CP-even
$\cos\theta_2^k$	B_2^k	b_k^-	P-odd, CP-even
$\cos\theta_1^r$	B_1^r	b_r^+	P-odd, CP-even
$\cos\theta_2^r$	B_2^r	b_r^-	P-odd, CP-even
$\cos\theta_1^n$	B_1^n	b_n^+	P-even, CP-even
$\cos\theta_2^n$	B_2^n	b_n^-	P-even, CP-even
$\cos\theta_1^{k*}$	B_1^{k*}	b_k^+	P-odd, CP-even
$\cos\theta_2^{k*}$	B_2^{k*}	b_k^-	P-odd, CP-even
$\cos\theta_1^{r*}$	B_1^{r*}	b_r^+	P-odd, CP-even
$\cos\theta_2^{r*}$	B_2^{r*}	b_r^-	P-odd, CP-even
$\cos\theta_1^k\cos\theta_2^k$	C_{kk}	c_{kk}	P-even, CP-even
$\cos\theta_1^r\cos\theta_2^r$	C_{rr}	c_{rr}	P-even, CP-even
$\cos\theta_1^n\cos\theta_2^n$	C_{nn}	c_{nn}	P-even, CP-even
$\cos\theta_1^r\cos\theta_2^k+\cos\theta_1^k\cos\theta_2^r$	$C_{rk}+C_{kr}$	c_{rk}	P-even, CP-even
$\cos\theta_1^r\cos\theta_2^k-\cos\theta_1^k\cos\theta_2^r$	$C_{rk}-C_{kr}$	c_n	P-even, CP-odd
$\cos\theta_1^n\cos\theta_2^r+\cos\theta_1^r\cos\theta_2^n$	$C_{nr}+C_{rn}$	c_{nr}	P-odd, CP-even
$\cos\theta_1^n\cos\theta_2^r-\cos\theta_1^r\cos\theta_2^n$	$C_{nr}-C_{rn}$	c_k	P-odd, CP-odd
$\cos\theta_1^n\cos\theta_2^k+\cos\theta_1^k\cos\theta_2^n$	$C_{nk}+C_{kn}$	c_{kn}	P-odd, CP-even
$\cos\theta_1^n\cos\theta_2^k-\cos\theta_1^k\cos\theta_2^n$	$C_{nk}-C_{kn}$	$-c_r$	P-odd, CP-odd
$\cos\varphi$	D	$-(c_{kk}+c_{rr}+c_{nn})/3$	P-even, CP-even
$\cos\varphi_{lab}$	$A_{\cos\varphi}^{lab}$	–	–
$\lvert\Delta\phi_{ll}\rvert$	$A_{\lvert\Delta\phi_{ll}\rvert}$	–	–

This can be simplified as the differential distribution of the cross-section. The cross section distribution for the double leptonic channel can be written as [71]

$$\frac{1}{\sigma}\frac{d^2\sigma}{d\cos\theta_1^i d\cos\theta_2^j}=\frac{1}{4}(1+B_1^i\cos\theta_1^i+B_2^j\cos\theta_2^j-C_{ij}\cos\theta_1^i\cos\theta_2^j) \tag{3.8}$$

where $\theta_1^i(\theta_2^j)$ is the angle between the direction of flight of the positively (negatively) charged lepton in the top quark (anti-quark) rest frame and the reference direction $\hat{a}$ ($\hat{b}$). The coefficients $B_{1,2}^{i,j}$ and C_{ij} in equation (3.8) reflect the properties of the spin density components in (3.3). The elements of $B_{1,2}$ and C matrices have the same discrete symmetry properties with related coefficient functions, see in table 3.2. To extract each coefficient separately one can reduce the double differential cross section in equation (3.8) to single differential distributions

$$\frac{1}{\sigma}\frac{d\sigma}{d\cos\theta_1^i}=\frac{1}{2}(1+B_1^i\cos\theta_1^i), \tag{3.9}$$

$$\frac{1}{\sigma}\frac{d\sigma}{d\cos\theta_2^i} = \frac{1}{2}(1+B_2^i\cos\theta_2^i), \tag{3.10}$$

$$\frac{1}{\sigma}\frac{d\sigma}{d(\cos\theta_1^i\cos\theta_2^i)} = \frac{1}{2}(1-C_{ii}\cos\theta_1^i\cos\theta_2^i)\ln\left(\frac{1}{|\cos\theta_1^i\cos\theta_2^i|}\right), \tag{3.11}$$

$$\frac{1}{\sigma}\frac{d\sigma}{dx_\pm} = \frac{1}{2}\left(1-\frac{C_{ij}\pm C_{ji}}{2}x_\pm\right)\cos^{-1}|x_\pm| \qquad (\text{for}\, i\neq j), \tag{3.12}$$

where $x_\pm = \cos\theta_1^i\cos\theta_2^j \pm \cos\theta_1^j\cos\theta_2^i$. In addition to equations (3.9) and (3.10), four further observables $\cos\theta_{1,2}^i$ with respect to modified axes $\hat{k}^*$ and $\hat{r}^*$ are calculated. Axes $\hat{k}^*$ and $\hat{r}^*$ for top quark are equal to $sign(\Delta|y|)\hat{k}$ and $sign(\Delta|y|)sign(\cos\Theta)\hat{r}$, respectively, while they are inverse for anti-top. Here $\Delta|y| = |y_t| - |y_{\bar{t}}|$ is the difference in absolute values of the rapidities of top and anti-top quarks in the laboratory frame. The observables in modified axes are sensitive to the NP contributions [15].

The opening angle $\cos\varphi$, which is obtained by the inner product of the direction of flight of positively and negatively charged leptons in their own top quark rest frames, is taken into account as a useful spin correlation observable below. The analysis also involves two observables measured directly in the laboratory-frame. First one is $\cos\varphi_{lab}$, which is defined as $\cos\varphi$ but in the laboratory-frame. $|\Delta\phi_{ll}|$ is the other observable measured in the laboratory-frame. It is the absolute azimuthal difference between the two charged leptons measured in the laboratory-frame. The observables measured in the laboratory-frame cannot be obtained from spin correlation or polarization observables, but they could have high precision in measurement and computation.

4. RESULTS AND INTERPRETATION

The aim of this chapter is to compare the samples simulated with different MC event generator configurations for spin correlation and polarization observables of top quark pairs at collision energy of 13 TeV. The sensitivity of the observables extracted from different MC event generator approaches is discussed. The statistical and systematic uncertainties on the distributions of the observables are presented to understand the deviations between predictions. Furthermore, all MC predictions are validaded with experimental data of CMS Collaboration.

The analysis can be separated into two parts as the investigation of the deviations of different MC event generator configurations on the distributions of the observables of $t\bar{t}$ events and the searching the new physics with these observables. Firstly, in the section 4.1, similar and unlike points in terms of the elements of spin density matrix in the SM $t\bar{t}$ samples are exhibited by taking into consideration systematic and statistical uncertainties. In addition, all theoretical predictions are compared with experimental results by considering limitations from experimental uncertainty.

The other side of the analysis is specifying the behaviour of some new physics models in the elements of the spin correlation matrix. The SUSY and the DM models have different shapes from SM $t\bar{t}$ in distributons of certain observables. Scalar particles in BSM models can effect the spin correlation of the top quark pairs. In the section 4.2, these effects will be discussed, and the BSM signals will be compared with predictions in SM $t\bar{t}$ and experimental data.

4.1 Theory-Data Comparison Analysis

In this section, the normalized differential distributions for the 22 observables mentioned in the previous chapter are presented as a comparison of various MC approaches and experimental measurements published by the CMS Collaboration [71]. The physics objects in events predicted by MC generators are considered at

generator-level. In that sense, objects come from MC history after decay but before hadronization. Last top quark in top quark decay chain as a top quark and first lepton after decay of W boson as a lepton are used in the calculations of observables. As leptons in dilepton events, prompt electrons and muons (not taus or decay products of taus) are taken into account.

Three different MC generators as MADGRAPH5_aMC@NLO, SHERPA and POWHEG BOX at LO and NLO QCD accuracy used in the analysis. As in the CMS analysis [71], the analysis with MC generators is in full phase space. As the nominal $t\bar{t}$ sample, we have been chosen the sample simulated by MADGRAPH5_aMC@NLO ME event generator at NLO interfaced with PYTHIA8 for the parton shower and fragmentation.

In figures 4.1-4.6, the differential distributions predicted by MADGRAPH5+PYTHIA8 at NLO is compared with MADGRAPH5+PYTHIA8 at LO accuracy, with POWHEG+PYTHIA8 at NLO, with SHERPA at LO, and with SHERPA at NLO QCD accuracy and at NLO in QCD with EW correction. To check the compatibility with experiment, all theoretical predictions are compared with CMS measurements. In the lower panels of the following figures, the ratio of the other predictions and the data to the nominal $t\bar{t}$ sample is shown with systematic and statistical uncertainties. The statistical uncertainty is specified with a grey band while the total uncertainty included the systematic and the statistical is yellow. The experimental uncertainty is given separately with the CMS data.

In figure 4.1, the diagonal spin correlation observables $\cos\theta_1^i \cos\theta_2^i$ defined in equation 3.11 are presented. The coefficient C_{rr} by considered QCD contributions at tree level has indeed a small value compared with the other P- and CP-even coefficients as seen in the figure, further details can be found in ref. [15]. There are no significant deviations in different MC approaches and different QCD corrections as well as EW correction. The experimental uncertainty comprise almost all variations of predictions.

The predictions for the differential distributions of the observables $x_{\pm}$, equation 3.12, are considered in figure 4.2. Non-zero coefficients $(C_{nr} + C_{rn})$ and $(C_{nk} + C_{kn})$ are expected from mixed QCD-weak corrections correspond to ref. [15]. Due to smallness of this effect, scale, PDF and experimental uncertainties dominate it. Within the

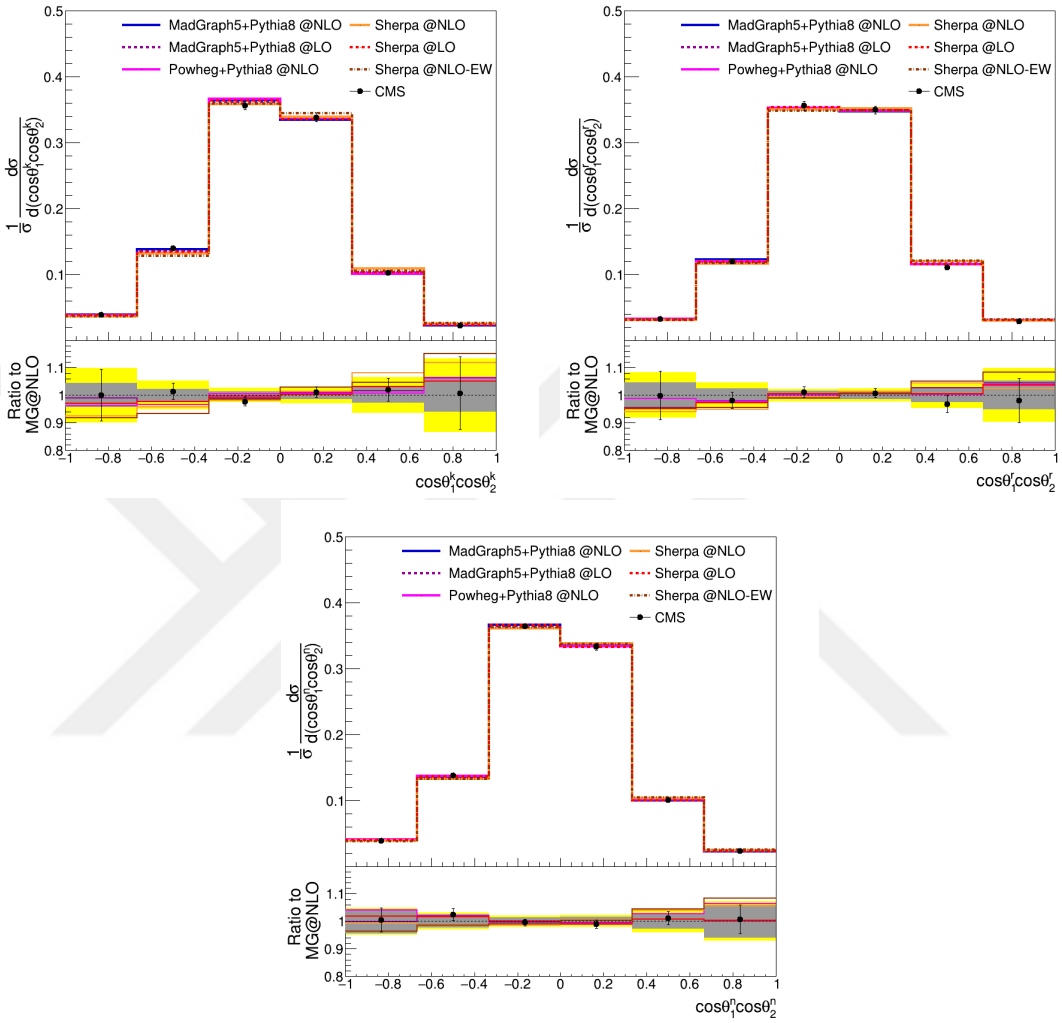

Figure 4.1 : The normalized differential cross sections with respect to the diagonal spin correlation observables $\cos\theta_1^i \cos\theta_2^i$, $i = k, r, n$ compared to the CMS data and the predictions from MADGRAPH5_aMC@NLO, SHERPA and POWHEG BOX in full phase space. The ratio of the normalized differential cross sections predicted by the other generator+parton shower configurations to MADGRAPH5+PYTHIA8 at NLO is shown in the lower panels. The statistical uncertainty band is shown in grey. The yellow uncertainty bands represent the overall uncertainty obtained by summing the systematic and statistical uncertainties in quadrature. The systematic uncertainty includes PDF and scale uncertainties.

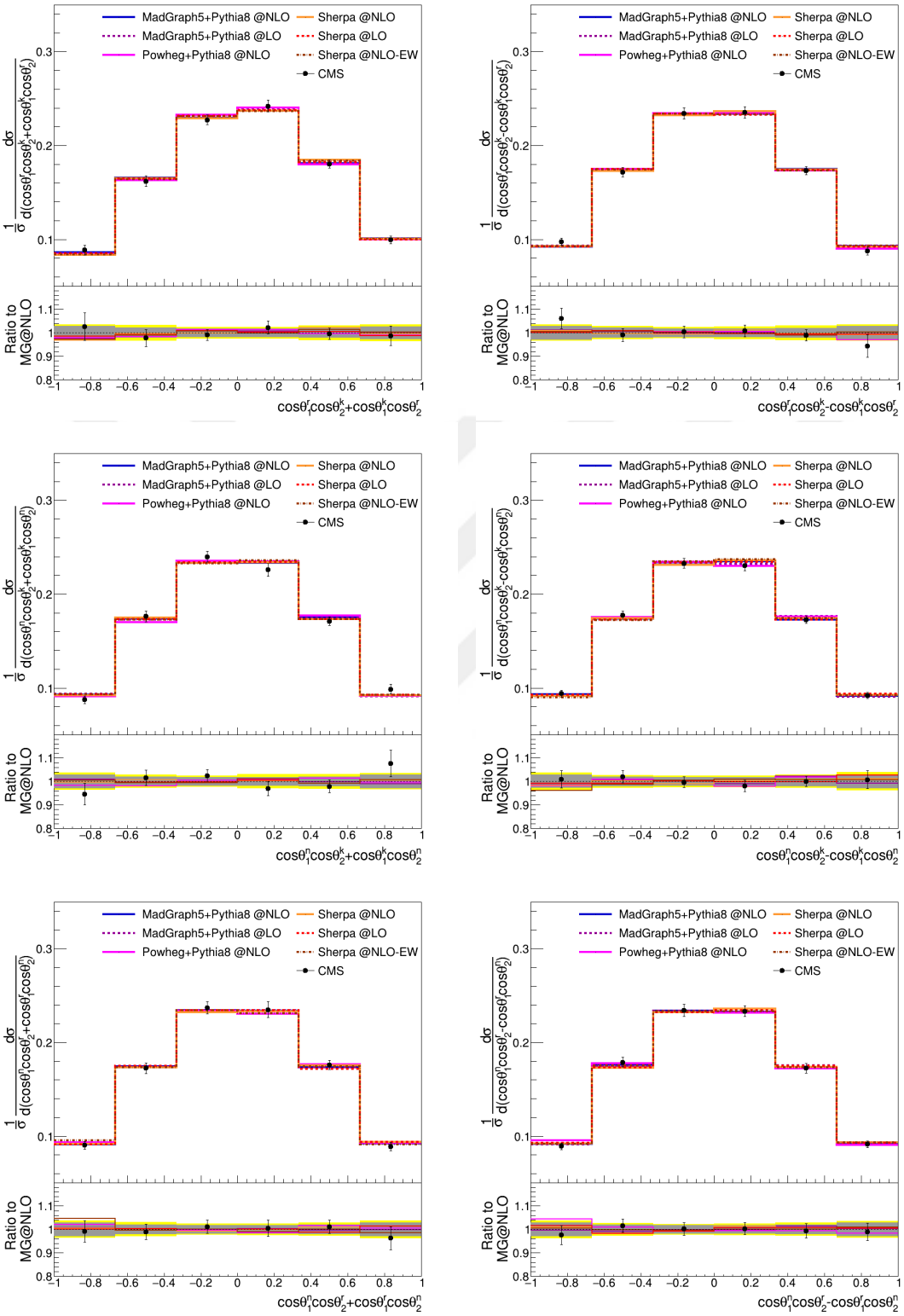

Figure 4.2 : The normalized differential cross sections with respect to the cross spin correlation observables $\cos\theta_1^i \cos\theta_2^j \pm \cos\theta_1^j \cos\theta_2^i$, $i \neq j$. The ratio panels compare the other predictions to nominal distribution.

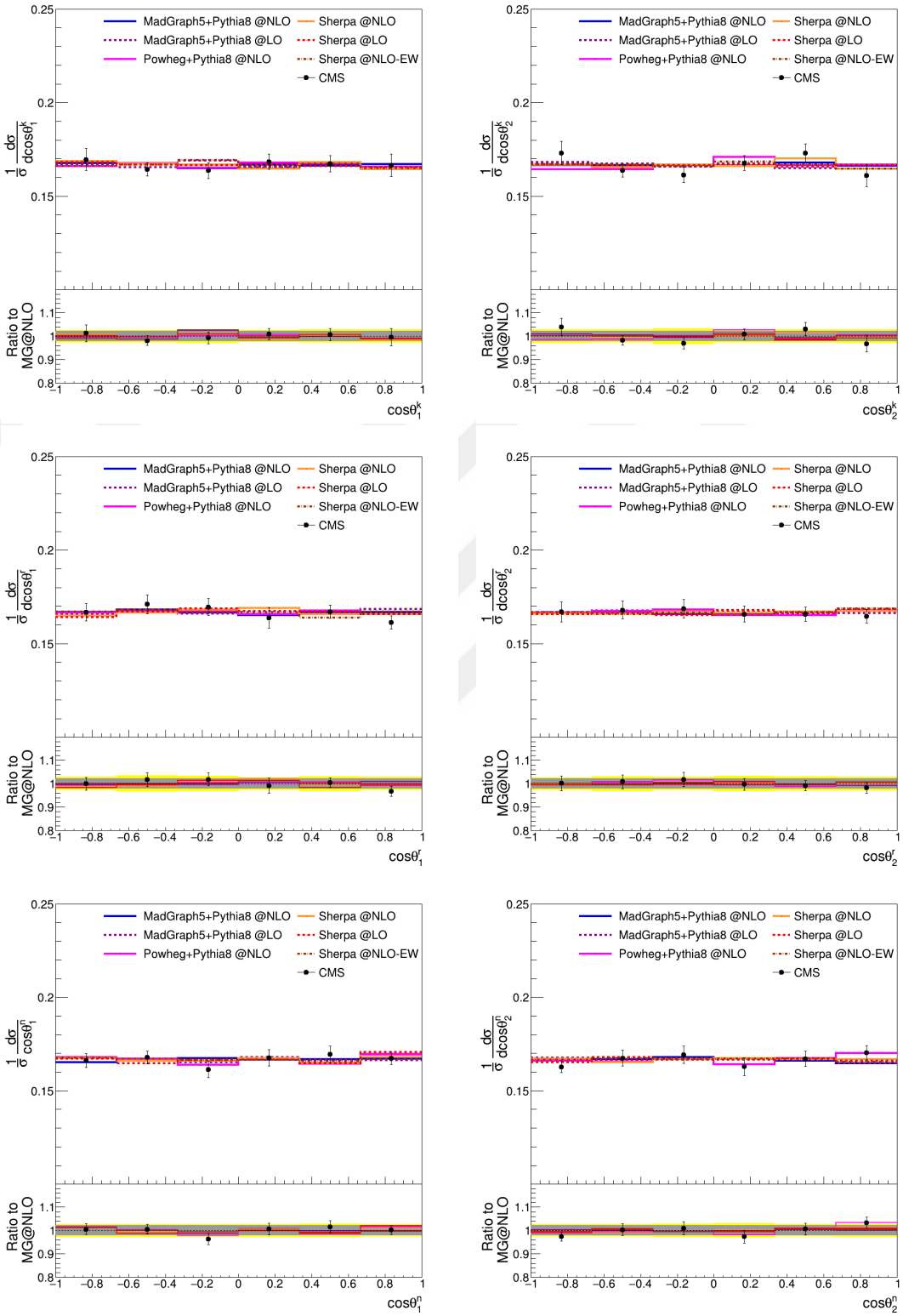

Figure 4.3 : The normalized differential cross sections with respect to the observables $\cos\theta_1^i$ and $\cos\theta_2^i$, $i = k, r, n$. The ratio panels compare the other predictions to nominal distribution.

uncertainties, the experimental data and predictions for cross diagonal spin correlation observables are match.

The normalized differential distributions in $\cos\theta^{i}_{1,2}$, equations (3.9, 3.10), which is the indicator of the polarization of top quark and anti-quark are shown in figure 4.3. The polarization coefficients for all predictions behave similar in all distributions. CMS data and MC predictions are compatible within uncertainties. In the same way, the normalized differential distributions of $\cos\theta^{i*}_{1,2}$ predicted by MC, figure 4.4, are in agreement with data.

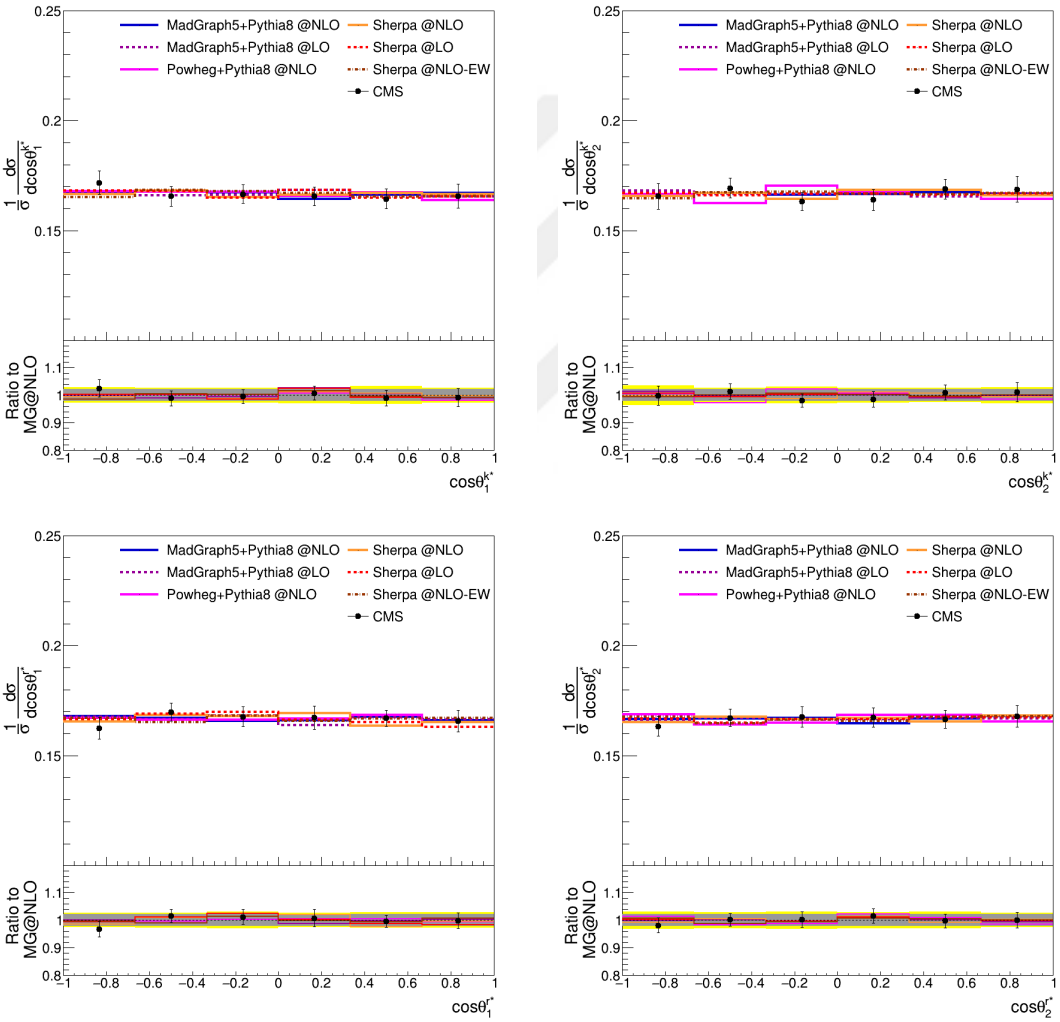

Figure 4.4 : The normalized differential cross sections with respect to the observables $\cos\theta^{i*}_{1}$ and $\cos\theta^{i*}_{2}$, $i = k, r, n$. The ratio panels compare the other predictions to nominal distribution.

The differential distributions in the observables, which are calculated with kinematic variables of leptons in laboratory-frame, are in figure 4.5. When $|\Delta\phi_{ll}|$ is considered with total uncertainty which is around 8%, the shapes predicted by MADGRAPH5

and Sherpa ME generators are roughly consistent. SHERPA and MADGRAPH5 at LO accuracy show better performance than the samples simulated at NLO due to real NLO contributions to $t\bar{t}$ processes. POWHEG is separated from the other MC predictions and the data about 10% at low and high $|\Delta\phi_{ll}|$ regions. For the distributions of $\cos\varphi_{lab}$, all MC predictions and tha data are in good agreement in whole range, although the systematic uncertainties coming from PDF sets and scales are more than 10% in almost whole regions. The huge systematic uncertainty as seen in the lower panel of the right plot in figure 4.5 is coming from PDF variations in SHERPA samples.

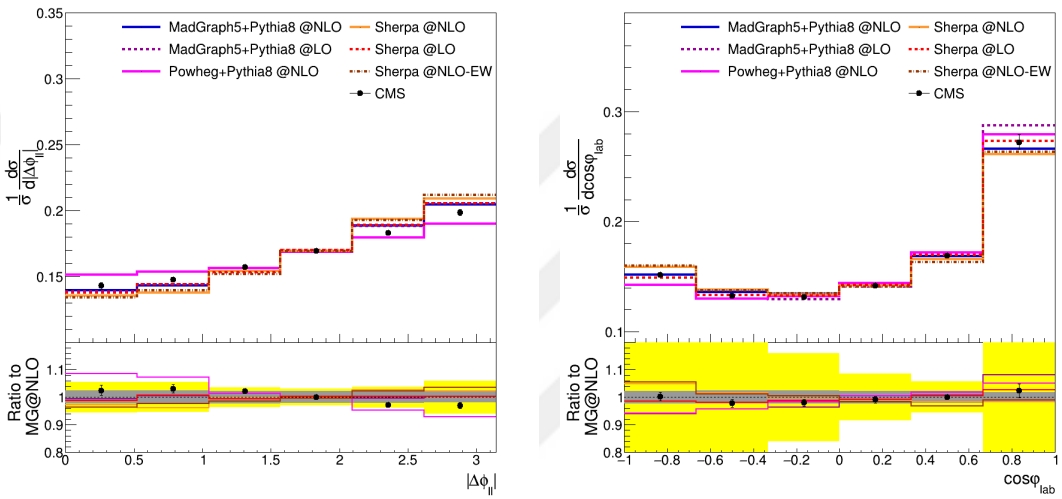

Figure 4.5 : The normalized differential cross section as a function of laboratory frame observable which are $|\Delta\phi_{ll}|$ (left plot) and $\cos\varphi_{lab}$ (right plot). The ratio panels compare the other predictions to nominal distribution.

In $\cos\varphi$ distribution, figure 4.6, the predictions of MC generators are more similar compared to laboratory-frame distributions. While the distributions of the most of variations of samples have quite same shape, SHERPA at NLO QCD accuracy and with EW correction deviate from others especially at low $\cos\varphi$.

4.2 Implications of Precision Measurements of Beyond the Standard Model

In this part of the analysis, it is investigated various new physics models with the help of the elements of spin density matrix. For top quark pair channel, most searches for SUSY and DM particles comprise generally high missing transverse energy E_T^{miss} region stem from undetected LSP and DM [17–20]. The main point for the BSM analysis in this study is the models with low E_T^{miss} but the same models with high E_T^{miss},

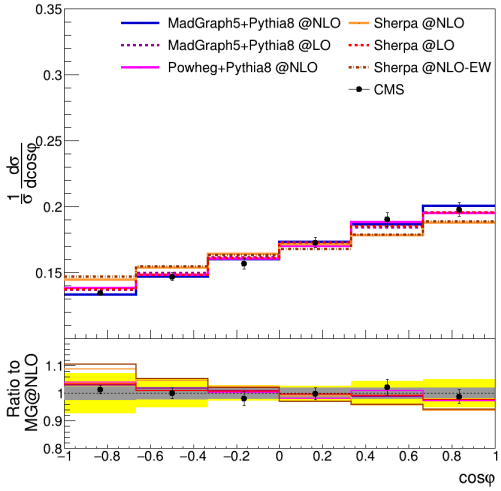

Figure 4.6 : The normalized differential cross section with respect to $\cos\varphi$ predicted by various MC event generators at LO, NLO and NLO-EW accuracy. The ratio of the other predictions to nominal distribution is shown in the lower panel.

which are not excluded by CMS and ATLAS Collaborations yet, will be mentioned for the sake of broad phase space.

As mentioned earlier, it will be taken into account three different BSM signals to compare with SM predicted results and the data. The details of the event samples of the signals can be seen in section 1.2. The SUSY samples were simulated as unpolarized. To check importance of it, the R-Parity conserved SUSY sample is determined as two separate configurations having polarized top squarks. To polarize the $\tilde{t}$ as fully left and right-handed, the distributions in the SUSY sample is multiplied by a weight obtained from the reweighting algorithm detailed in [76]. The second signal is that DM model having scalar or pseudoscalar mediator associated with top quark pair. Within this model, the collision process has missing transverse energy E_T^{miss} as in the model above. For both sample, the study is focused on a narrow phase space in which mass difference between $\tilde{t}$ and $\tilde{\chi}_1^0$ is slightly bigger than top or the mediator mass is relatively small, in this case 10 GeV. To ensure the larger phase space in the $\tilde{t}$ mass, the R-Parity violating (RPV) SUSY is included in the analysis framework. The mechanism of the R-Parity violation gives us three quarks decayed from $\tilde{\chi}_1^0$. Thus E_T^{miss} in the $\tilde{t}$ pair production consists of only neutrinos from top quark decay chain. The following results for RPV SUSY are performed with a signal point of $m_{\tilde{t}} = 400$ GeV, for the details, the rest of the phase space is given in the Appendix B.

The distributions of spin correlation and polarization observables are presented in figures 4.7-4.12. The figures involve related BSM signals, CMS data and the nominal $t\bar{t}$ sample with systematic and statistical uncertainty calculated as in the previous section. In the lower panels, the statistical uncertainties of the signals are specified on each signal sample.

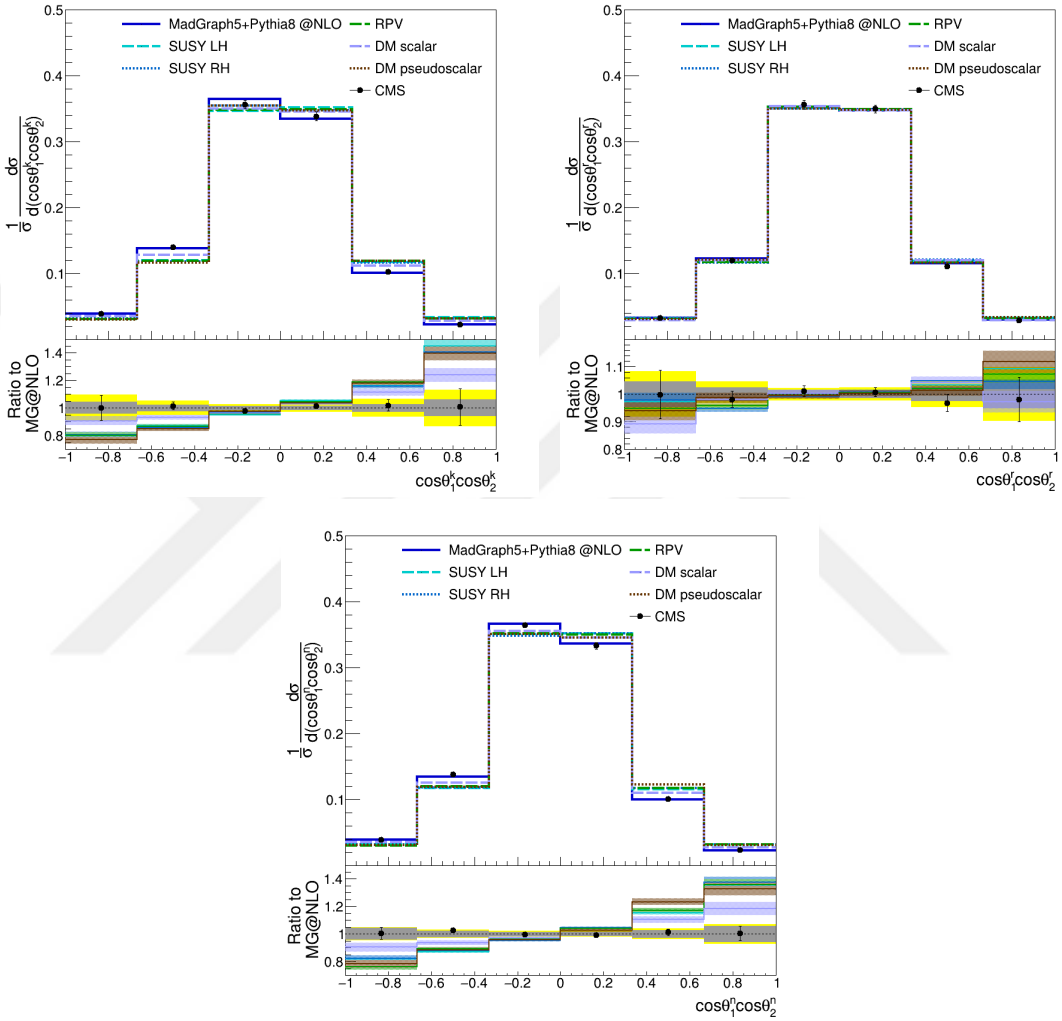

Figure 4.7 : The normalized differential cross sections with respect to the diagonal spin correlation observables $\cos\theta_1^i\cos\theta_2^i$, $i = k, r, n$ compared to the nominal $t\bar{t}$ sample, the CMS data and the BSM signals. The statistical uncertainty band of the SM $t\bar{t}$ samples is shown in grey. The yellow uncertainty bands represent the overall uncertainty obtained by summing the systematic and statistical uncertainties of the SM $t\bar{t}$ samples in quadrature. The statistical uncertainties of the signals are specified on each signal sample.

The differential distributions of the diagonal spin correlation observables in BSM signals are shown in figure 4.7. Almost all signals for $\cos\theta_1^k\cos\theta_2^k$ and $\cos\theta_1^n\cos\theta_2^n$ observables deviate up to 40% from SM nominal $t\bar{t}$ predictions and the CMS data. For

$\cos\theta_1^r \cos\theta_2^r$, the difference between signals and the nominal sample is can be seen despite the domination of the uncertainties. It is seen that the scalar-mediated DM signal apart from the others has a non-zero diagonal spin correlation coefficient.

In figure 4.8, the distributions of the observables $x_\pm$ defined in equation 3.12 are discussed for signals with the nominal $t\bar{t}$ sample and the CMS data. The distribution in the upper left corner has a difference between signals and nominal sample because the coefficient of this observable is generated by P and CP conserving interactions as in the diagonal spin coefficients. For the other cross spin correlation observables, the distributions of signals and the nominal $t\bar{t}$ sample are compatible with the experimental data when considered total uncertainty.

The observables in equations (3.9, 3.10) are not sensitive to small amount of top quark polarization predicted in both BSM and SM as seen in figures 4.9-4.10. The distributions are very flat for all predictions and the data. Furthermore, polarized stops do not have any effect on the distributions as shown in fully left and right-handed separated SUSY samples.

The laboratory frame observables are indicator of presence of spin correlations as in P- and CP-even observables. Especially the $|\Delta\phi_{ll}|$ distribution in figure 4.11 reveals this with the difference between BSM and SM. Moreover, it can be seen that the dark matter model with scalar mediator has spin correlation though not as much as SM. In the $\cos\varphi_{lab}$ with high systematic uncertainties, some BSM models act as in the SM while others deviate much more.

The last spin correlation sensitive observable is that the inner product of flight direction of two leptons in its own top quark center of mass frame ($\cos\varphi$). In the figure 4.12, the sensitivity to spin correlation is seen in the DM with scalar mediator while not in the other BSM samples.

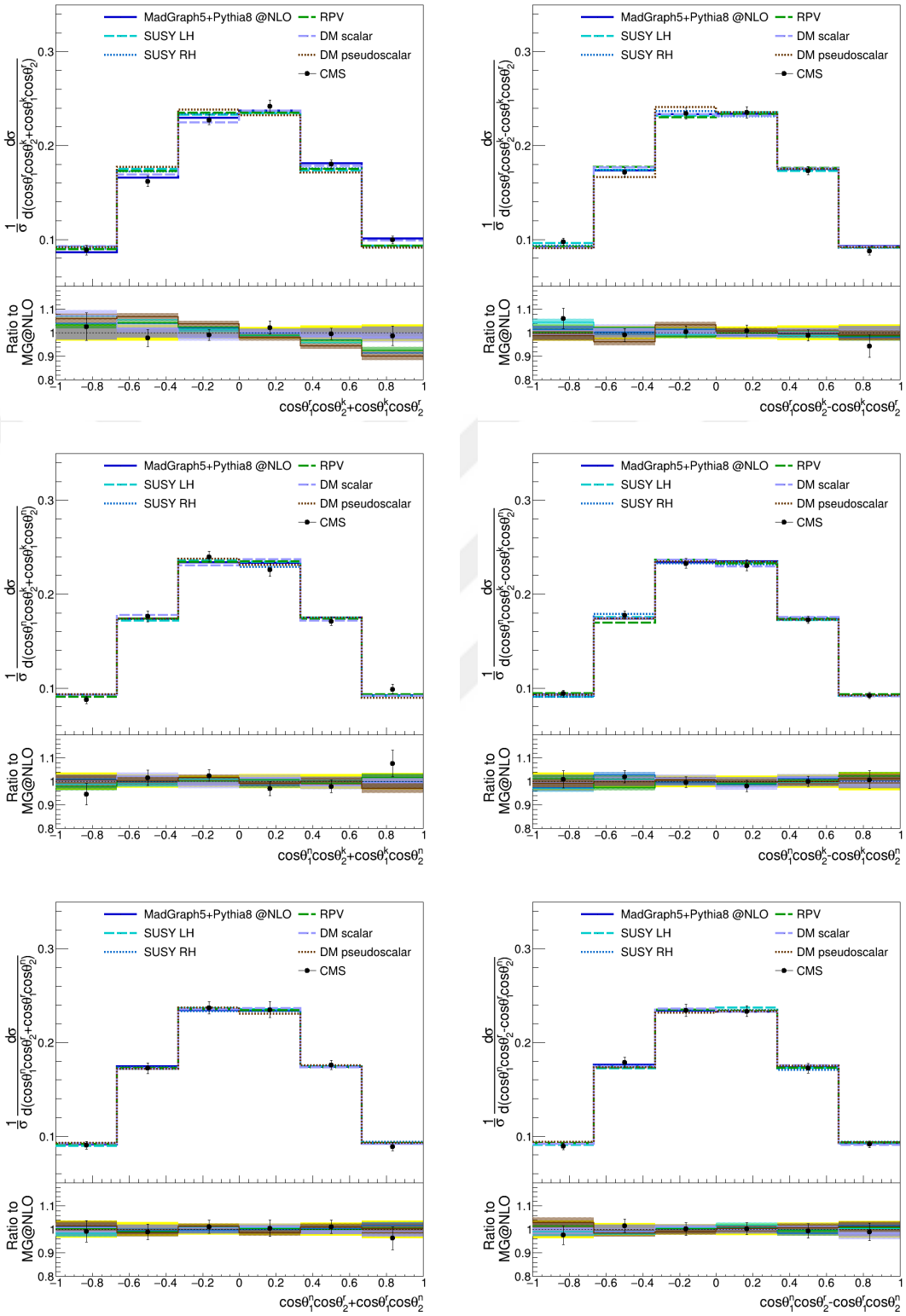

Figure 4.8 : The normalized differential cross sections with respect to the cross spin correlation observables $\cos\theta_1^i \cos\theta_2^j \pm \cos\theta_1^j \cos\theta_2^i$, $i \neq j$. The ratio panels compare the BSM signals to the nominal distribution.

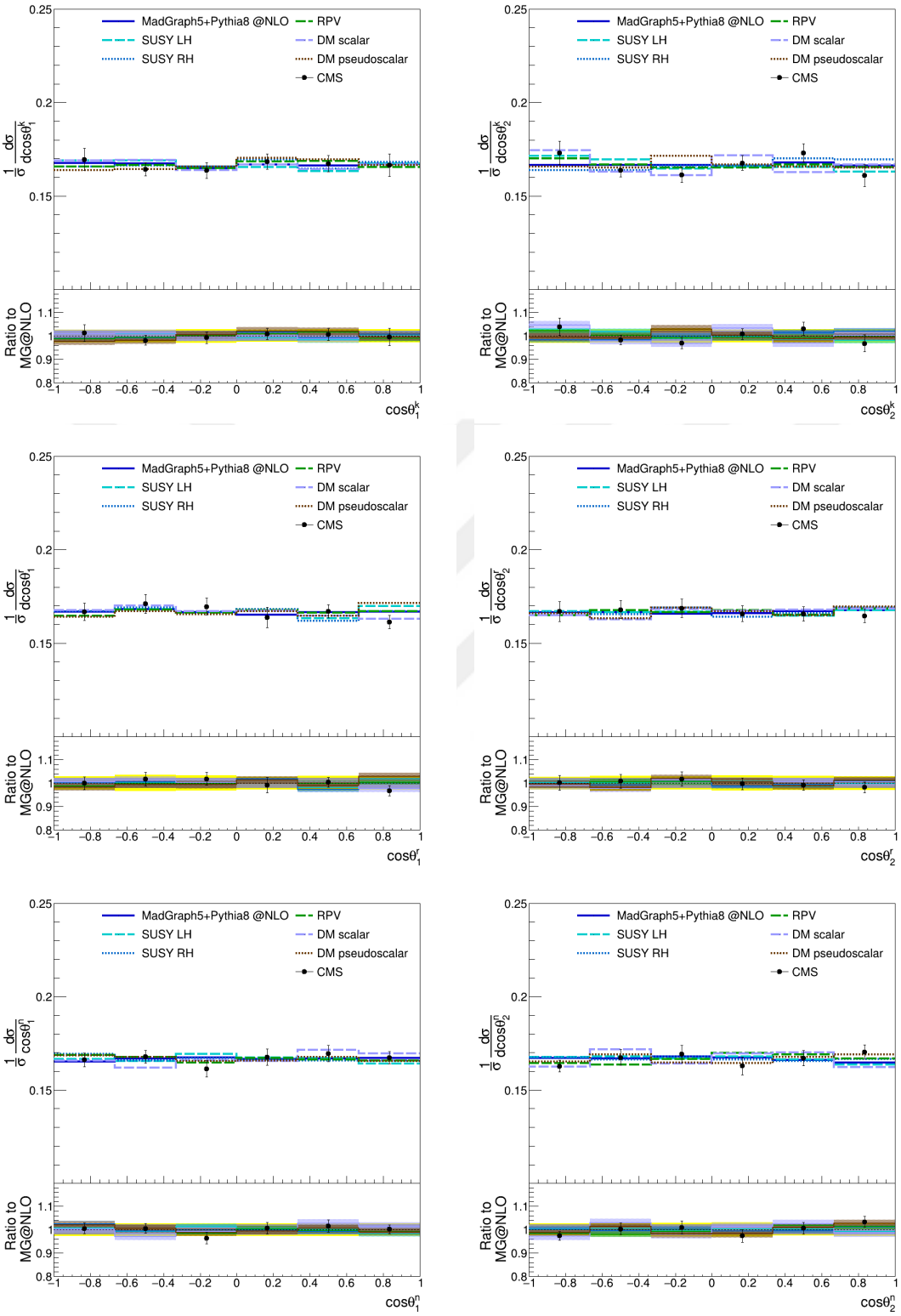

Figure 4.9 : The normalized differential cross sections with respect to the observables $\cos\theta_1^i$ and $\cos\theta_2^i$, $i = k, r, n$. The ratio panels compare the BSM signals to the nominal distribution.

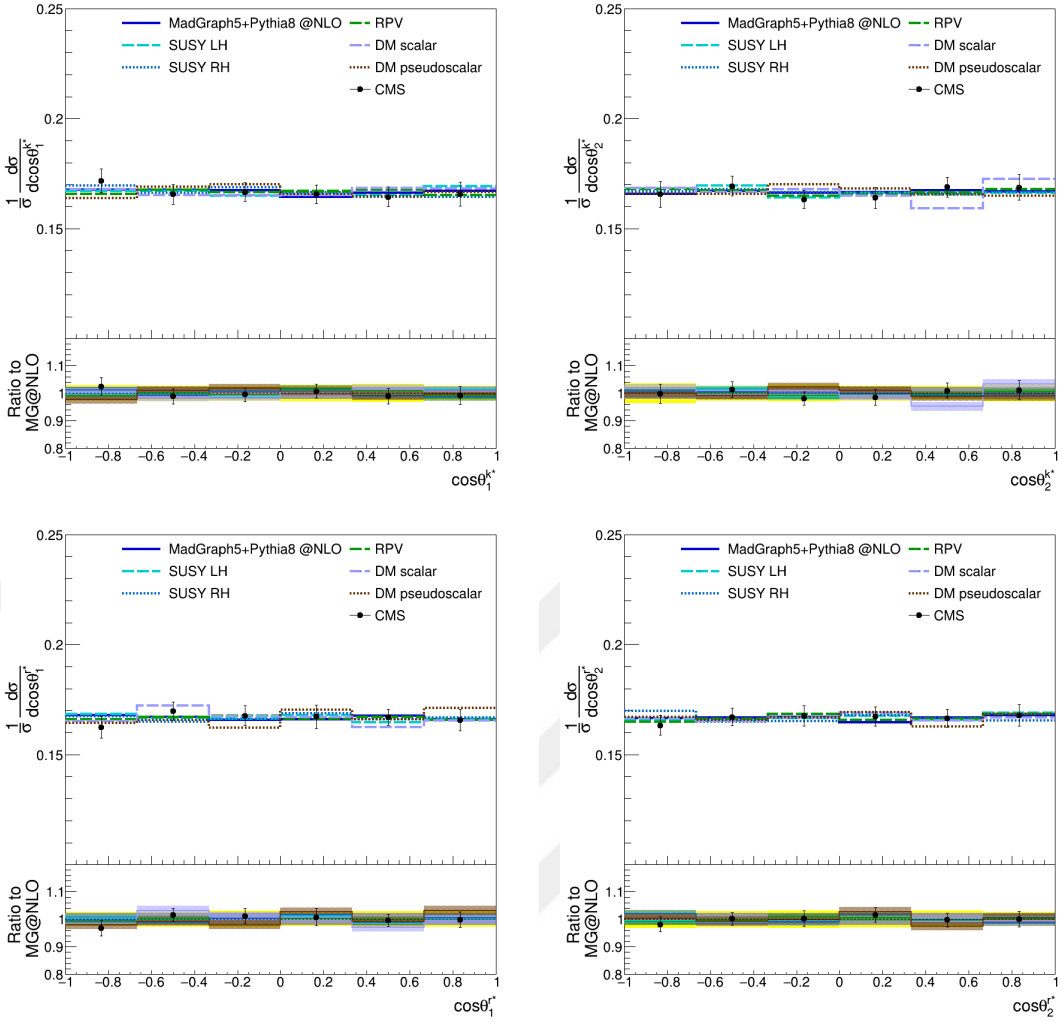

Figure 4.10 : The normalized differential cross sections with respect to the observables $\cos\theta_1^{i*}$ and $\cos\theta_2^{i*}$, $i = k, r, n$. The ratio panels compare the BSM signals to the nominal distribution.

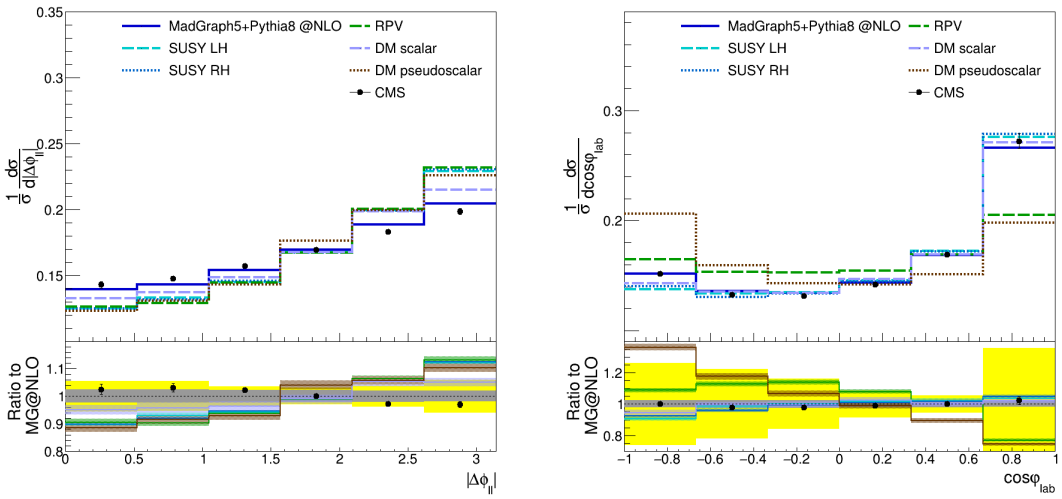

Figure 4.11 : The normalized differential cross section as a function of laboratory frame observable which are $|\Delta\phi_{ll}|$ (left plot) and $\cos\varphi_{lab}$ (right plot).The ratio panels compare the BSM signals to the nominal distribution.

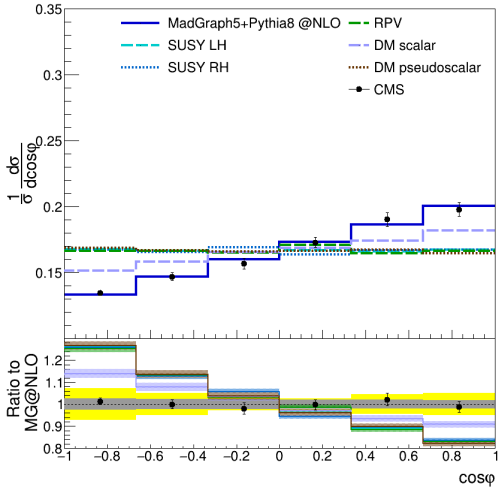

Figure 4.12 : The normalized differential cross section with respect to $\cos\varphi$. The ratio panel compares the BSM signals to the nominal distribution.

5. CONCLUSION AND OUTLOOK

The standard model is a powerful theory that has been verified many times by many experiments. While it has fascinating achievements, it is fact that the SM is an incomplete theory. Shedding light on the inconsistencies in the experiments and finding new interactions arising from as yet possible undiscovered particles make the precise measurement of the SM inevitable. With its unique properties, the top quark has a key role in precision measurements. The strong Yukawa coupling of the top quark to the Higgs boson makes it important for measuring the properties of the Higgs boson and even other particles in the SM. In addition to being the heaviest elementary particle, the top quark quickly decays to other particles, so the spin information is transferred to the decay products without spoiling. This property allows us to investigate possible spin correlation and polarization of top quarks in pair production. The observable coefficients from the $t\bar{t}$ production spin density matrix decomposition present a detailed analysis of the top quark spin properties.

As mentioned above, the SM has inconsistencies with some phenomenological studies and theoretical expectations. Various models such as SUSY have been developed to overcome the issues in the SM. SUSY is a theory accepted by many physicists, but no signs have been found so far. Numerous studies to search for a SUSY signature are based on the missing transverse energy coming from neutralinos. Separating the SUSY signal from $t\bar{t}$ background in a region of low missing transverse energy is a challenging task, due to similarities of momentum topologies. At this point, precision measurements gain importance, one of those is spin correlation and polarization of top-quark pairs.

To make predictions for $t\bar{t}$ production and to simulate the SUSY signals, Monte Carlo event generators are necessary tools. By ATLAS and CMS Collaborations in high energy processes, mostly used ones are MADGRAPH5_aMC@NLO, SHERPA and POWHEG, and are interfaced with PYTHIA8 to generate parton showers. However, SHERPA is a general purpose event generator so it has its own parton shower

module. In this thesis, $t\bar{t}$ samples were produced in different MC event generator configurations and discussed for top quark pair spin correlations and polarizations. Considering the different configurations, the polarization terms and the cross terms of the spin correlation observables are in agreement within the systematic and statistical uncertainty. Especially samples of SHERPA at NLO accuracy (and with electroweak corrections) for diagonal terms in the spin correlation observables tend to deviate from others but are still in total uncertainty. The biggest contribution to the uncertainty comes from the PDF variations of predictions at LO accuracy. Separation can be seen better in NLO calculations due to the less dependency of higher order calculations to the PDF variations. Furthermore, to be more accurate in predictions, it is needed to increase the statistics in experimental data. The behavior of the different configurations can be clearly seen in the $\cos\varphi$ and $|\Delta\phi_{ll}|$ distributions, the observables most sensitive to spin correlation in the top quark pair. The deviations up to 10% in SHERPA samples for these observables, in figures 4.11 and 4.12, could be arisen from its approximation in hard and large angle emissions.

For the BSM signals having low missing transverse energy, spin correlation observables provide good separation. The diagonal spin correlation observables having the largest absolute value show discrepancy up to 40% between signals and nominal $t\bar{t}$ prediction except dark matter sample with a scalar mediator. Only the DM sample with a scalar mediator has spin correlation, unlike other BSM signals, but the spin correlation power in its top-quark pair is not as much as in the SM. Furthermore, polarized stop quarks of different composition have no impact on top quark spin correlation.

The different MC event generator configurations are compatible with each other, within total uncertainty, for the observables of spin correlation and polarization in the top quark pair. However, for some observables as mentioned above, there are small separations dominated by systematic uncertainties. NNLO calculations can make these differences more visible by reducing systematic uncertainties, or they can reduce the difference between configurations by making more accurate calculations with higher-order ME calculations. Thereby, this gets NNLO calculations for theoretical predictions more important. Additionally, the observables may be used, especially

in low missing transverse energy region, for searching BSM signals due to their sensitivity of contributions from parity and/or CP conserving or violating interactions.

REFERENCES

[1] **Commons, W.** (2021). (Online accessed: 28 June, 2021), https://commons.wikimedia.org/w/index.php?title=File:Elementary_particle_interactions.svgoldid=551305552.

[2] **Kumericki, K.**, (2016), Feynman Diagrams for Beginners, `Arxiv:1602.04182`.

[3] **Quadt, A.** (2007). *Top quark physics at hadron colliders*, Springer Berlin Heidelberg, Berlin, Heidelberg.

[4] **Gleisberg, T.**, **Höche, S.**, **Krauss, F.**, **Schönherr, M.**, **Schumann, S.**, **Siegert, F. and Winter, J.** (2009). Event generation with SHERPA 1.1, *Journal of High Energy Physics*, *2009*(02), 007–007.

[5] **Webber, B.R.** (2000). Fragmentation and hadronization, *Int. J. Mod. Phys. A*, *15S1*, 577–606, `Arxiv:hep-ph/9912292`.

[6] **Cabibbo, N.** (1963). Unitary Symmetry and Leptonic Decays, *Phys. Rev. Lett.*, *10*, 531–533.

[7] **Kobayashi, M. and Maskawa, T.** (1973). CP-Violation in the Renormalizable Theory of Weak Interaction, *Progress of Theoretical Physics*, *49*(2), 652–657.

[8] **Abulencia, A.** *et al.* (2007). Precision measurement of the top quark mass from dilepton events at CDF II, *Phys. Rev. D*, *75*, 031105, `Arxiv:hep-ex/0612060`.

[9] **Abazov, V.M.** *et al.* (2015). Precision measurement of the top-quark mass in lepton+jets final states, *Phys. Rev. D*, *91*(11), 112003, `Arxiv:1501.07912`.

[10] **Collaboration, A.** (2021). *Top quark precision measurements with the ATLAS experiment at the LHC*, cern document server. Retrieved May 30, 2021, from https://cds.cern.ch/record/2767499.

[11] **Aad, G.** *et al.* (2020). Test of the universality of τ and μ lepton couplings in W-boson decays from $t\bar{t}$ events with the ATLAS detector, `Arxiv:2007.14040`.

[12] **Maes, M.** (2012). *Measurement of the Top Quark mass and other properties with CMS*, cern document server. Retrieved May 15, 2021, from http://cds.cern.ch/record/1478224.

[13] **Mahlon, G. and Parke, S.J.** (1996). Angular correlations in top quark pair production and decay at hadron colliders, *Phys. Rev. D*, *53*, 4886–4896, `Arxiv:hep-ph/9512264`.

[14] **Bernreuther, W.**, **Brandenburg, A.**, **Si, Z.G. and Uwer, P.** (2001). Top-Quark Spin Correlations at Hadron Colliders: Predictions at Next-to-Leading Order QCD, *Physical Review Letters*, *87*(24).

[15] **Bernreuther, W.**, **Heisler, D. and Si, Z.G.** (2015). A set of top quark spin correlation and polarization observables for the LHC: Standard Model predictions and new physics contributions, *Journal of High Energy Physics*, *2015*(12), 1–36.

[16] **Czakon, M. and Mitov, A.** (2014). Top++: A Program for the Calculation of the Top-Pair Cross-Section at Hadron Colliders, *Comput. Phys. Commun.*, *185*, 2930, `Arxiv:1112.5675`.

[17] **Sirunyan, A.M.**, **Tumasyan, A.**, **Adam, W.**, **Ambrogi, F.**, **Asilar, E.**, **Bergauer, T.**, **Brandstetter, J.**, **Dragicevic, M.**, **Erö, J. and et al.** (2019). Search for the pair production of light top squarks in the $e-mu$ final state in proton-proton collisions at $\sqrt{s} = 13$ TeV, *Journal of High Energy Physics*, *2019*(3).

[18] **Aaboud, M.**, **Aad, G.**, **Abbott, B.**, **Abdinov, O.**, **Abeloos, B.**, **Abidi, S.H.**, **AbouZeid, O.S.**, **Abraham, N.L.**, **Abramowicz, H. and et al.** (2017). Search for direct top squark pair production in final states with two leptons in $\sqrt{s} = 13$ TeV pp collisions with the ATLAS detector, *The European Physical Journal C*, *77*(12).

[19] **Aaboud, M.** *et al.* (2020). Measurements of top-quark pair spin correlations in the $e\mu$ channel at $\sqrt{s} = 13$ TeV using pp collisions in the ATLAS detector, *Eur. Phys. J. C*, *80*(8), 754, `Arxiv:1903.07570`.

[20] **Aad, G.** *et al.* (2021). Search for new phenomena in events with two opposite-charge leptons, jets and missing transverse momentum in pp collisions at $\sqrt{s}$ = 13 TeV with the ATLAS detector, *JHEP*, *04*, 165, `Arxiv:2102.01444`.

[21] **Farrar, G.R. and Fayet, P.** (1978). Phenomenology of the Production, Decay, and Detection of New Hadronic States Associated with Supersymmetry, *Phys. Lett. B*, *76*, 575–579.

[22] **Barbier, R.**, **Bérat, C.**, **Besançon, M.**, **Chemtob, M.**, **Deandrea, A.**, **Dudas, E.**, **Fayet, P.**, **Lavignac, S.**, **Moreau, G.**, **Perez, E. and et al.** (2005). R-Parity-violating supersymmetry, *Physics Reports*, *420*(1-6), 1–195.

[23] **Collaboration, C.**, (2021), Search for top squarks in final states with two top quarks and several light-flavor jets in proton-proton collisions at $\sqrt{s} =$ 13 TeV, `Arxiv:2102.06976`.

[24] **Peskin, M.E. and Schroeder, D.V.** (1995). *An Introduction to quantum field theory*, Addison-Wesley, Reading, USA.

[25] **Kluge, W.** (2008). Initial State Radiation: A Success story, *Nucl. Phys. B Proc. Suppl.*, *181-182*, 280–285, `Arxiv:0805.4708`.

[26] **Mrenna, S. and Richardson, P.** (2004). Matching matrix elements and parton showers with HERWIG and PYTHIA, *JHEP*, *05*, 040, `Arxiv:hep-ph/0312274`.

[27] **Fadin, V.S.**, **Lipatov, L.N.**, **Martin, A.D. and Melles, M.** (2000). Resummation of double logarithms in electroweak high energy processes, *Physical Review D*, *61*(9).

[28] **Mishra, K.**, **Barzè, L.**, **Becher, T.**, **Chiesa, M.**, **Dittmaier, S.**, **i Tormo, X.G.**, **Huss, A.**, **Kasprzik, T.**, **Li, Y.**, **Montagna, G. and et al.**, (2013), Electroweak Corrections at High Energies, `Arxiv:1308.1430`.

[29] **Gell-Mann, M.** (1964). A Schematic Model of Baryons and Mesons, *Phys. Lett.*, *8*, 214–215.

[30] **Chaichian, M. and Nishijima, K.** (1999). An Essay on color confinement, `Arxiv:hep-th/9909158`.

[31] **Collins, J.C.**, **Soper, D.E. and Sterman, G.F.** (1989). Factorization of Hard Processes in QCD, *Adv. Ser. Direct. High Energy Phys.*, *5*, 1–91, `Arxiv:hep-ph/0409313`.

[32] **Collins, J.** (2013). *Foundations of perturbative QCD*, (Vol 32), Cambridge University Press.

[33] **Lai, H.L.**, **Guzzi, M.**, **Huston, J.**, **Li, Z.**, **Nadolsky, P.M.**, **Pumplin, J. and Yuan, C.P.** (2010). New parton distributions for collider physics, *Physical Review D*, *82*(7).

[34] **Harland-Lang, L.A.**, **Martin, A.D.**, **Motylinski, P. and Thorne, R.S.** (2015). Parton distributions in the LHC era: MMHT 2014 PDFs, *The European Physical Journal C*, *75*(5).

[35] **Ball, R.D.**, **Bertone, V.**, **Carrazza, S.**, **Deans, C.S.**, **Del Debbio, L.**, **Forte, S.**, **Guffanti, A.**, **Hartland, N.P.**, **Latorre, J.I. and et al.** (2015). Parton distributions for the LHC run II, *Journal of High Energy Physics*, *2015*(4).

[36] **Buckley, A.**, **Butterworth, J.**, **Gieseke, S.**, **Grellscheid, D.**, **Höche, S.**, **Hoeth, H.**, **Krauss, F.**, **Lönnblad, L.**, **Nurse, E.**, **Richardson, P. and et al.** (2011). General-purpose event generators for LHC physics, *Physics Reports*, *504*(5), 145–233.

[37] **Sjöstrand, T.**, **Mrenna, S. and Skands, P.** (2008). A brief introduction to PYTHIA 8.1, *Computer Physics Communications*, *178*(11), 852–867.

[38] **Berends, F. and Giele, W.** (1988). Recursive calculations for processes with n gluons, *Nuclear Physics B*, *306*(4), 759–808.

[39] **Draggiotis, P.**, **Kleiss, R. and Papadopoulos, C.** (2002). Multi-jet production in hadron collisions, *The European Physical Journal C*, *24*(3), 447–458.

[40] **Campbell, J.M. and Ellis, R.K.** (1999). Update on vector boson pair production at hadron colliders, *Physical Review D*, *60*(11).

[41] **Campbell, J.M. and Ellis, R.K.** (2015). Top-Quark Processes at NLO in Production and Decay, *J. Phys. G*, *42*(1), 015005, `Arxiv:1204.1513`.

[42] **Campbell, J.M. and Ellis, R.** (2010). MCFM for the Tevatron and the LHC, *Nuclear Physics B - Proceedings Supplements*, *205-206*, 10–15.

[43] **Campbell, J.M.**, **Ellis, R.K.**, **Nason, P. and Re, E.** (2015). Top-pair production and decay at NLO matched with parton showers, *Journal of High Energy Physics*, *2015*(4).

[44] **Sjöstrand, T.**, **Ask, S.**, **Christiansen, J.R.**, **Corke, R.**, **Desai, N.**, **Ilten, P.**, **Mrenna, S.**, **Prestel, S.**, **Rasmussen, C.O. and Skands, P.Z.** (2015). An introduction to PYTHIA 8.2, *Computer Physics Communications*, *191*, 159–177.

[45] **Catani, S. and Seymour, M.** (1997). A general algorithm for calculating jet cross sections in NLO QCD, *Nuclear Physics B*, *485*(1-2), 291–419.

[46] **Schumann, S. and Krauss, F.** (2008). A parton shower algorithm based on Catani-Seymour dipole factorisation, *Journal of High Energy Physics*, *2008*(03), 038–038.

[47] **Bothmann, E.**, **Singh Chahal, G.**, **Höche, S.**, **Krause, J.**, **Krauss, F.**, **Kuttimalai, S.**, **Liebschner, S.**, **Napoletano, D.**, **Schönherr, M.**, **Schulz, H. and et al.** (2019). Event generation with Sherpa 2.2, *SciPost Physics*, *7*(3).

[48] **Höche, S. and Prestel, S.** (2015). The midpoint between dipole and parton showers, *The European Physical Journal C*, *75*(9).

[49] **Webber, B.R.** (1984). A QCD Model for Jet Fragmentation Including Soft Gluon Interference, *Nucl. Phys. B*, *238*, 492–528.

[50] **Andersson, B.**, **Mohanty, S. and Soderberg, F.** (2002). Recent developments in the Lund model, *36th Annual Winter School on Nuclear and Particle Physics (PINP 2002) and 8th St. Petersburg School on Theoretical Physics*, `Arxiv:hep-ph/0212122`.

[51] **Ovyn, S.**, **Rouby, X. and Lemaitre, V.** (2009). DELPHES, a framework for fast simulation of a generic collider experiment, `Arxiv:0903.2225`.

[52] **Brun, R.**, **Rademakers, F.**, **Canal, P.**, **Naumann, A.**, **Couet, O.**, **Moneta, L.**, **Vassilev, V.**, **Linev, S.**, **Piparo, D.**, **GANIS, G.**, **and et al.**, (2019), root-project/root: v6.18/02, `doi:10.5281/zenodo.3895860`.

[53] **de Favereau, J.**, **Delaere, C.**, **Demin, P.**, **Giammanco, A.**, **Lemaître, V.**, **Mertens, A. and Selvaggi, M.** (2014). DELPHES 3: a modular framework for fast simulation of a generic collider experiment, *Journal of High Energy Physics*, *2014*(2).

[54] **Alwall, J.**, **Frederix, R.**, **Frixione, S.**, **Hirschi, V.**, **Maltoni, F.**, **Mattelaer, O.**, **Shao, H.S.**, **Stelzer, T.**, **Torrielli, P. and Zaro, M.** (2014). The automated computation of tree-level and next-to-leading order differential cross sections, and their matching to parton shower simulations, *Journal of High Energy Physics*, *2014*(7).

[55] **Hoeche, S.**, **Krauss, F.**, **Lavesson, N.**, **Lonnblad, L.**, **Mangano, M.**, **Schalicke, A. and Schumann, S.** (2005). Matching parton showers and matrix elements, *HERA and the LHC: A Workshop on the Implications of HERA for LHC Physics: CERN - DESY Workshop 2004/2005*, `Arxiv:hep-ph/0602031`.

[56] **Frederix, R. and Frixione, S.** (2012). Merging meets matching in MC@NLO, *Journal of High Energy Physics*, *2012*(12).

[57] **Gleisberg, T. and Höche, S.** (2008). Comix, a new matrix element generator, *Journal of High Energy Physics*, *2008*(12), 039–039.

[58] **Buccioni, F.**, **Lang, J.N.**, **Lindert, J.M.**, **Maierhöfer, P.**, **Pozzorini, S.**, **Zhang, H. and Zoller, M.F.** (2019). OpenLoops 2, *The European Physical Journal C*, *79*(10).

[59] **Cascioli, F.**, **Maierhöfer, P. and Pozzorini, S.** (2012). Scattering Amplitudes with Open Loops, *Physical Review Letters*, *108*(11).

[60] **Denner, A.**, **Dittmaier, S. and Hofer, L.** (2017). Collier: A fortran-based complex one-loop library in extended regularizations, *Computer Physics Communications*, *212*, 220–238.

[61] **Höche, S.**, **Schumann, S. and Siegert, F.** (2010). Hard photon production and matrix-element parton-shower merging, *Physical Review D*, *81*(3).

[62] **Höche, S.**, **Krauss, F.**, **Schönherr, M. and Siegert, F.** (2013). QCD matrix elements + parton showers. The NLO case, *Journal of High Energy Physics*, *2013*(4).

[63] **Frixione, S. and Webber, B.R.** (2002). Matching NLO QCD computations and parton shower simulations, *Journal of High Energy Physics*, *2002*(06), 029–029.

[64] **Frixione, S.**, **Ridolfi, G. and Nason, P.** (2007). A positive-weight next-to-leading-order Monte Carlo for heavy flavour hadroproduction, *Journal of High Energy Physics*, *2007*(09), 126–126.

[65] **Nason, P.** (2004). A New Method for Combining NLO QCD with Shower Monte Carlo Algorithms, *Journal of High Energy Physics*, *2004*(11), 040–040.

[66] **Frixione, S.**, **Nason, P. and Oleari, C.** (2007). Matching NLO QCD computations with parton shower simulations: the POWHEG method, *Journal of High Energy Physics*, *2007*(11), 070–070.

[67] **Alioli, S.**, **Nason, P.**, **Oleari, C. and Re, E.** (2010). A general framework for implementing NLO calculations in shower Monte Carlo programs: the POWHEG BOX, *Journal of High Energy Physics*, *2010*(6).

[68] **Ball, R.D.**, **Bertone, V.**, **Carrazza, S.**, **Debbio, L.D.**, **Forte, S.**, **Groth-Merrild, P.**, **Guffanti, A.**, **Hartland, N.P.**, **Kassabov, Z.**, **Latorre, J.I. and et al.** (2017). Parton distributions from high-precision collider data, *The European Physical Journal C*, *77*(10).

[69] **Buckley, A.**, **Ferrando, J.**, **Lloyd, S.**, **Nordström, K.**, **Page, B.**, **Rüfenacht, M.**, **Schönherr, M. and Watt, G.** (2015). LHAPDF6: parton density access in the LHC precision era, *The European Physical Journal C*, *75*(3).

[70] **Collaboration, A.** (2017). *Studies on top-quark Monte Carlo modelling with Sherpa and MG5_aMC@NLO*, cern document server. Retrieved April 12, 2021, from http://cds.cern.ch/record/2261938.

[71] **Sirunyan, A.**, **Tumasyan, A.**, **Adam, W.**, **Ambrogi, F.**, **Asilar, E.**, **Bergauer, T.**, **Brandstetter, J.**, **Dragicevic, M.**, **Erö, J.**, **Escalante Del Valle, A. and et al.** (2019). Measurement of the top quark polarization and $t\bar{t}$ spin correlations using dilepton final states in proton-proton collisions at s=13 TeV, *Physical Review D*, *100*(7).

[72] **Bernreuther, W. and Brandenburg, A.** (1994). TracingCPviolation in the production of top quark pairs by multiple TeV proton-proton collisions, *Physical Review D*, *49*(9), 4481–4492.

[73] **Bernreuther, W.**, **Brandenburg, A.**, **Si, Z. and Uwer, P.** (2004). Top quark pair production and decay at hadron colliders, *Nuclear Physics B*, *690*(1-2), 81–137.

[74] **Melnikov, K. and Schulze, M.** (2009). NLO QCD corrections to top quark pair production and decay at hadron colliders, *Journal of High Energy Physics*, *2009*(08), 049–049.

[75] **Aguilar-Saavedra, J.**, **Carvalho, J.**, **Castro, N.**, **Onofre, A. and Veloso, F.** (2007). Probing anomalous Wtb couplings in top pair decays, *The European Physical Journal C*, *50*(3), 519–533.

[76] **Cms-Sus-Xpag**. *Stop reweighting*, retrieved May 10, 2021, from https://github.com/CMS-SUS-XPAG/Stop_reweight.

APPENDICES

APPENDIX A : Data cards used in Monte Carlo event generators
APPENDIX B : RPV SUSY model with different stop masses

APPENDIX A

The data cards used to produce $t\bar{t}$ events in Monte Carlo event generators are given below.

Proc card for the MADGRAPH5_aMC@NLO:

```
#*********************************************************
#*                       MadGraph5_aMC@NLO               *
#*                                                       *
#*                 *                       *             *
#*                   *        * *        *               *
#*                     * * * * 5 * * * *                 *
#*                   *        * *        *               *
#*                 *                       *             *
#*                                                       *
#*                                                       *
#*          VERSION 2.6.6                 2018-06-28     *
#*                                                       *
#*     The MadGraph5_aMC@NLO Development Team - Find us at *
#*     https://server06.fynu.ucl.ac.be/projects/madgraph *
#*                                                       *
#*********************************************************
#*                                                       *
#*                Command File for MadGraph5_aMC@NLO     *
#*                                                       *
#*      run as ./bin/mg5_aMC  filename                   *
#*                                                       *
#*********************************************************
set default_unset_couplings 99
set group_subprocesses Auto
set ignore_six_quark_processes False
set loop_optimized_output True
set low_mem_multicore_nlo_generation False
set loop_color_flows False
set gauge unitary
set complex_mass_scheme False
set max_npoint_for_channel 0
import model sm
define p = g u c d s u~ c~ d~ s~
define j = g u c d s u~ c~ d~ s~
define l+ = e+ mu+
define l- = e- mu-
define vl = ve vm vt
define vl~ = ve~ vm~ vt~
set low_mem_multicore_nlo_generation True
set nb_core 10
import model loop_sm
generate p p > t t~ [QCD] @0
add process p p > t t~ j [QCD] @1
add process p p > t t~ j j [QCD] @2
output /afs/cern.ch/work/o/okolay/private/MadGraph5_events/nnpdf30_2j_\
spin_dilepton_m1725
```

Run card for the MADGRAPH5_aMC@NLO:

```
#*********************************************************************
#                          MadGraph5_aMC@NLO                         *
#                                                                    *
#                       run_card.dat aMC@NLO                         *
#                                                                    *
#  This file is used to set the parameters of the run.               *
#                                                                    *
#  Some notation/conventions:                                        *
#                                                                    *
#   Lines starting with a hash (#) are info or comments              *
#                                                                    *
#   mind the format:   value    = variable     ! comment             *
#                                                                    *
#   Some of the values of variables can be list. These can either be *
#   comma or space separated.                                        *
#                                                                    *
#   To display additional parameter, you can use the command:        *
#      update to_full                                                *
#*********************************************************************
#
#*******************
# Running parameters
#*******************
#
#*********************************************************************
# Tag name for the run (one word)                                    *
#*********************************************************************
  tag_1 = run_tag ! name of the run
#*********************************************************************
# Number of LHE events (and their normalization) and the required    *
# (relative) accuracy on the Xsec.                                   *
# These values are ignored for fixed order runs                      *
#*********************************************************************
  150000        = nevents ! Number of unweighted events requested
  -1.0  = req_acc ! Required accuracy (-1=auto determined from nevents)
  -1    = nevt_job ! Max number of events per job in event generation.
                 ! (-1= no split).
#*********************************************************************
# Normalize the weights of LHE events such that they sum or average to *
# the total cross section                                            *
#*********************************************************************
  average       = event_norm ! valid settings: average, sum, bias
#*********************************************************************
# Number of points per itegration channel (ignored for aMC@NLO runs)  *
#*********************************************************************
  0.01  = req_acc_fo ! Required accuracy (-1=ignored, and use the
                           ! number of points and iter. below)
# These numbers are ignored except if req_acc_FO is equal to -1
  5000  = npoints_fo_grid ! number of points to setup grids
  4     = niters_fo_grid ! number of iter. to setup grids
  10000 = npoints_fo ! number of points to compute Xsec
  6     = niters_fo ! number of iter. to compute Xsec
#*********************************************************************
# Random number seed                                                 *
#*********************************************************************
  6124  = iseed ! rnd seed (0=assigned automatically=default))
#*********************************************************************
# Collider type and energy                                           *
#*********************************************************************
  1     = lpp1 ! beam 1 type (0 = no PDF)
  1     = lpp2 ! beam 2 type (0 = no PDF)
  6500.0        = ebeam1 ! beam 1 energy in GeV
  6500.0        = ebeam2 ! beam 2 energy in GeV
#*********************************************************************
# PDF choice: this automatically fixes also alpha_s(MZ) and its evol.  *
#*********************************************************************
  lhapdf        = pdlabel ! PDF set
  260000        = lhaid ! If pdlabel=lhapdf, this is the lhapdf number. Only
              ! numbers for central PDF sets are allowed. Can be a list;
              ! PDF sets beyond the first are included via reweighting.
#*********************************************************************
# Include the NLO Monte Carlo subtr. terms for the following parton    *
```

```
# shower (HERWIG6 | HERWIGPP | PYTHIA6Q | PYTHIA6PT | PYTHIA8)          *
# WARNING: PYTHIA6PT works only for processes without FSR!!!!           *
#*********************************************************************
  PYTHIA8        = parton_shower
  1.0    = shower_scale_factor ! multiply default shower starting
                                 ! scale by this factor
#*********************************************************************
# Renormalization and factorization scales                             *
# (Default functional form for the non-fixed scales is the sum of      *
# the transverse masses divided by two of all final state particles    *
# and partons. This can be changed in SubProcesses/set_scales.f or via *
# dynamical_scale_choice option)                                       *
#*********************************************************************
  False = fixed_ren_scale ! if .true. use fixed ren scale
  False = fixed_fac_scale ! if .true. use fixed fac scale
  91.118         = mur_ref_fixed ! fixed ren reference scale
  91.118         = muf_ref_fixed ! fixed fact reference scale
  -1     = dynamical_scale_choice ! Choose one (or more) of the predefined
           ! dynamical choices. Can be a list; scale choices beyond the
           ! first are included via reweighting
  1.0    = mur_over_ref ! ratio of current muR over reference muR
  1.0    = muf_over_ref ! ratio of current muF over reference muF
#*********************************************************************
# Reweight variables for scale dependence and PDF uncertainty          *
#*********************************************************************
  1.0, 2.0, 0.5 = rw_rscale ! muR factors to be included by reweighting
  1.0, 2.0, 0.5 = rw_fscale ! muF factors to be included by reweighting
  True   = reweight_scale ! Reweight to get scale variation using the
           ! rw_rscale and rw_fscale factors. Should be a list of
           ! booleans of equal length to dynamical_scale_choice to
           ! specify for which choice to include scale dependence.
  False = reweight_pdf ! Reweight to get PDF uncertainty. Should be a
           ! list booleans of equal length to lhaid to specify for
           !  which PDF set to include the uncertainties.
#*********************************************************************
# Store reweight information in the LHE file for off-line model-       *
# parameter reweighting at NLO+PS accuracy                             *
#*********************************************************************
  False = store_rwgt_info ! Store info for reweighting in LHE file
#*********************************************************************
# ickkw parameter:                                                     *
#    0: No merging                                                     *
#    3: FxFx Merging - WARNING! Applies merging only at the hard-event *
#       level. After showering an MLM-type merging should be applied as *
#       well. See http://amcatnlo.cern.ch/FxFx_merging.htm for details. *
#    4: UNLOPS merging (with pythia8 only). No interface from within   *
#       MG5_aMC available, but available in Pythia8.                  *
#   -1: NNLL+NLO jet-veto computation. See arxiv:1412.8408 [hep-ph].   *
#*********************************************************************
  3      = ickkw
#*********************************************************************
#
#*********************************************************************
# BW cutoff (M+/-bwcutoff*Gamma). Determines which resonances are      *
# written in the LHE event file                                        *
#*********************************************************************
  15.0   = bwcutoff
#*********************************************************************
# Cuts on the jets. Jet clustering is performed by FastJet.            *
#  - When matching to a parton shower, these generation cuts should be *
#    considerably softer than the analysis cuts.                       *
#  - More specific cuts can be specified in SubProcesses/cuts.f        *
#*********************************************************************
  1.0    = jetalgo ! FastJet jet algorithm (1=kT, 0=C/A, -1=anti-kT)
  1.0    = jetradius ! The radius parameter for the jet algorithm
  20.0   = ptj ! Min jet transverse momentum
  -1.0   = etaj ! Max jet abs(pseudo-rap) (a value .lt.0 means no cut)
#*********************************************************************
# Cuts on the charged leptons (e+, e-, mu+, mu-, tau+ and tau-)        *
# More specific cuts can be specified in SubProcesses/cuts.f           *
#*********************************************************************
  0.0    = ptl ! Min lepton transverse momentum
  -1.0   = etal ! Max lepton abs(pseudo-rap) (a value .lt.0 means no cut)
  0.0    = drll ! Min distance between opposite sign lepton pairs
```

```
  0.0    = drll_sf ! Min distance between opp. sign same-flavor lepton pairs
  0.0    = mll ! Min inv. mass of all opposite sign lepton pairs
  30.0   = mll_sf ! Min inv. mass of all opp. sign same-flavor lepton pairs
#*********************************************************************
# Photon-isolation cuts, according to hep-ph/9801442. When ptgmin=0,   *
# all the other parameters are ignored.                               *
# More specific cuts can be specified in SubProcesses/cuts.f          *
#*********************************************************************
  20.0   = ptgmin ! Min photon transverse momentum
  -1.0   = etagamma ! Max photon abs(pseudo-rap)
  0.4    = r0gamma ! Radius of isolation code
  1.0    = xn ! n parameter of eq.(3.4) in hep-ph/9801442
  1.0    = epsgamma ! epsilon_gamma parameter of eq.(3.4) in hep-ph/9801442
  True   = isoem ! isolate photons from EM energy (photons and leptons)
#*********************************************************************
# Cuts associated to MASSIVE particles identified by their PDG codes.  *
# All cuts are applied to both particles and anti-particles, so use    *
# POSITIVE PDG CODES only. Example of the syntax is {6 : 100} or       *
# {6:100, 25:200} for multiple particles                              *
#*********************************************************************
  {}     = pt_min_pdg ! Min pT for a massive particle
  {}     = pt_max_pdg ! Max pT for a massive particle
  {}     = mxx_min_pdg ! inv. mass for any pair of (anti)particles
#*********************************************************************
# For aMCfast+APPLGRID use in PDF fitting (http://amcfast.hepforge.org)*
#*********************************************************************
  0      = iappl ! aMCfast switch (0=OFF, 1=prepare grids, 2=fill grids)
#*********************************************************************
#*******************************************************************
#  Additional hidden parameters
#*******************************************************************
  False = fixed_qes_scale # hidden_parameter
```

Parameter card for the MADGRAPH5_aMC@NLO:

```
######################################################################
## PARAM_CARD AUTOMATICALY GENERATED BY MG5 FOLLOWING UFO MODEL    ####
######################################################################
##                                                                  ##
##  Width set on Auto will be computed following the information    ##
##        present in the decay.py files of the model.               ##
##        See  arXiv:1402.1178 for more details.                    ##
##                                                                  ##
######################################################################

###################################
## INFORMATION FOR LOOP
###################################
Block loop
    1 9.118800e+01 # MU_R

###################################
## INFORMATION FOR MASS
###################################
Block mass
    5 4.700000e+00 # MB
    6 1.725000e+02 # MT
   15 1.777000e+00 # MTA
   23 9.118800e+01 # MZ
   25 1.250000e+02 # MH
## Dependent parameters, given by model restrictions.
## Those values should be edited following the
## analytical expression. MG5 ignores those values
## but they are important for interfacing the output of MG5
## to external program such as Pythia.
  1 0.000000e+00 # d : 0.0
  2 0.000000e+00 # u : 0.0
  3 0.000000e+00 # s : 0.0
  4 0.000000e+00 # c : 0.0
  11 0.000000e+00 # e- : 0.0
  12 0.000000e+00 # ve : 0.0
  13 0.000000e+00 # mu- : 0.0
  14 0.000000e+00 # vm : 0.0
```

```
  16 0.000000e+00 # vt : 0.0
  21 0.000000e+00 # g : 0.0
  22 0.000000e+00 # a : 0.0
  24 8.041900e+01 # w+ : cmath.sqrt(MZ__exp__2/2. + cmath.sqrt(MZ__exp__4/4. \
  - (aEW*cmath.pi*MZ__exp__2)/(Gf*sqrt__2)))

###################################
## INFORMATION FOR SMINPUTS
###################################
Block sminputs
     1 1.325070e+02 # aEWM1
     2 1.166390e-05 # Gf
     3 1.180000e-01 # aS

###################################
## INFORMATION FOR YUKAWA
###################################
Block yukawa
     5 4.700000e+00 # ymb
     6 1.730000e+02 # ymt
    15 1.777000e+00 # ymtau

###################################
## INFORMATION FOR DECAY
###################################
DECAY    6 1.491500e+00 # WT
DECAY   23 2.441404e+00 # WZ
DECAY   24 2.047600e+00 # WW
DECAY   25 6.382339e-03 # WH
## Dependent parameters, given by model restrictions.
## Those values should be edited following the
## analytical expression. MG5 ignores those values
## but they are important for interfacing the output of MG5
## to external program such as Pythia.
DECAY   1 0.000000e+00 # d : 0.0
DECAY   2 0.000000e+00 # u : 0.0
DECAY   3 0.000000e+00 # s : 0.0
DECAY   4 0.000000e+00 # c : 0.0
DECAY   5 0.000000e+00 # b : 0.0
DECAY   11 0.000000e+00 # e- : 0.0
DECAY   12 0.000000e+00 # ve : 0.0
DECAY   13 0.000000e+00 # mu- : 0.0
DECAY   14 0.000000e+00 # vm : 0.0
DECAY   15 0.000000e+00 # ta- : 0.0
DECAY   16 0.000000e+00 # vt : 0.0
DECAY   21 0.000000e+00 # g : 0.0
DECAY   22 0.000000e+00 # a : 0.0
#=========================================================
# QUANTUM NUMBERS OF NEW STATE(S) (NON SM PDG CODE)
#=========================================================

Block QNUMBERS 82  # gh
        1 0  # 3 times electric charge
        2 1  # number of spin states (2S+1)
        3 8  # colour rep (1: singlet, 3: triplet, 8: octet)
        4 1  # Particle/Antiparticle distinction (0=own anti)
```

Run card for SHERPA:

```
(run){
  EVENTS 1000;

  % scales, tags for scale variations
  FSF:=1.; RSF:=1.; QSF:=1.;
  SCALE_VARIATIONS 0.25,0.25 0.25,1. 0.25,4. 1.,0.25 1.,1. 1.,4. 4.,0.25 4.,1. 4.,4.;
  ASSOCIATED_CONTRIBUTIONS_VARIATIONS=EW EW|LO1 EW|LO1|LO2 EW|LO1|LO2|LO3;
  CORE_SCALE VAR{sqr(172.5)+0.5*(PPerp2(p[2])+PPerp2(p[3]))};
  EXCLUSIVE_CLUSTER_MODE 1;
  METS_BBAR_MODE 5;

  % tags for process setup
  NJET:=3; LJET:=2,3; QCUT:=30.;

```

```
  % me generator settings
  ME_SIGNAL_GENERATOR Comix Amegic LOOPGEN;
  OL_PREFIX=/afs/cern.ch/work/o/okolay/private/Frameworks/OpenLoops/OpenLoops-2.0.0;
  LOOPGEN:=OpenLoops;
  MI_HANDLER=Amisic;
  EVENT_GENERATION_MODE Unweighted;
  NLO_SMEAR_THRESHOLD 1;
  NLO_SMEAR_POWER 2;

  % collider setup
  BEAM_1=2212;
  BEAM_2=2212;
  BEAM_ENERGY_1=6500;
  BEAM_ENERGY_2=6500;

  % decays
  HARD_DECAYS On; HARD_SPIN_CORRELATIONS 1;
  SOFT_SPIN_CORRELATIONS=1;
  %SPECIAL_TAU_SPIN_CORRELATIONS=1;
  HEPMC_USE_NAMED_WEIGHTS 1;
  HDH_STATUS[24,12,-11]=2;
  HDH_STATUS[24,14,-13]=2;
  HDH_STATUS[24,16,-15]=2;
  HDH_STATUS[-24,-12,11]=2;
  HDH_STATUS[-24,-14,13]=2;
  HDH_STATUS[-24,-16,15]=2;

  PDF_LIBRARY LHAPDFSherpa;
  PDF_SET NNPDF30_nlo_as_0118;
  PDF_VARIATIONS CT10nlo[all] MMHT2014nlo68cl[all] NNPDF30_nlo_as_0118[all];
  RESULT_DIRECTORY res_proc1;
  USE_PDF_ALPHAS=1;

  MAX_PROPER_LIFETIME=10.0;
  HEPMC_TREE_LIKE=1;
  PRETTY_PRINT=Off;
  MASS[6]=172.5;
  STABLE[6]=0;
  WIDTH[6]=0;
  MASS[15]=1.777;
  WIDTH[15]=2.26735e-12;
  MASS[23]=91.1876;
  WIDTH[23]=0;
  MASS[24]=80.399;
  STABLE[24]=0;
  WIDTH[24]=0;
  SIN2THETAW=0.23113;


  OL_PARAMETERS=preset=2;
  OL_PARAMETERS=write_parameters=1;
  OL_PARAMETERS=ew_scheme 2 ew_renorm_scheme 1;
}(run)
(processes){
  Process : 93 93 -> 6 -6 93{NJET};
  Order (*,0); CKKW sqr(QCUT/E_CMS);
  NLO_QCD_Mode MC@NLO {LJET};
  ME_Generator Amegic {LJET};
  RS_ME_Generator Comix {LJET};
  Loop_Generator LOOPGEN {LJET};
  Associated_Contributions EW|LO1|LO2|LO3 {LJET};
  Max_N_Quarks 6 {5,6,7,8};
  Integration_Error 0.05 {5,6,7,8};
}(processes)
```

Input card for POWHEG:

```
! TTbar production parameters
!randomseed 352345 ! uncomment to set the random seed to a value of your choice.
                   ! It generates the call RM48IN(352345,0,0) (see the RM48 manual).
                   ! THIS MAY ONLY AFFECTS THE GENERATION OF POWHEG EVENTS!
                   ! If POWHEG is interfaced to a shower MC, refer to the shower MC
                   ! documentation to set its seed.
```

```
!Heavy flavour production parameters

numevts NEVENTS
iseed SEED
ih1   1         ! hadron 1
ih2   1         ! hadron 2
#ndns1 131       ! pdf for hadron 1 (hvqpdf numbering)
#ndns2 131       ! pdf for hadron 2
! To be set only if using LHA pdfs
lhans1 260000        ! pdf set for hadron 1 (LHA numbering)
lhans2 260000        ! pdf set for hadron 2 (LHA numbering)
! To be set only if using different pdf sets for the two incoming hadrons
! QCDLambda5  0.25 ! for not equal pdf sets
ebeam1 6500     ! energy of beam 1
ebeam2 6500     ! energy of beam 2
qmass  172.5      ! mass of heavy quark in GeV
facscfact 1     ! factorization scale factor: mufact=muref*facscfact
renscfact 1     ! renormalization scale factor: muren=muref*renscfact
#fixedscale 1     ! use ref. scale=qmass (default 0, use running scale)
hdamp 272.7225

topdecaymode 20000   ! an integer of 5 digits that are either 0, or 2, representing in
                     ! the order the maximum number of the following particles
                     ! (antiparticles) in the final state: e  mu tau up charm
                     ! For example
                     ! 22222    All decays (up to 2 units of everything)
                     ! 20000    both top go into b l nu (with the appropriate signs)
                     ! 10011    one top goes into electron (or positron), the other
                     !           into (any) hadrons, or one top goes into charm, the
                     !           other into up
                     ! 00022    Fully hadronic
                     ! 00002    Fully hadronic with two charms
                     ! 00011    Fully hadronic with a single charm
                     ! 00012    Fully hadronic with at least one charm

!semileptonic 1      ! uncomment if you want to filter out only semileptonic events.
                     ! For example, with topdecaymode 10011 and semileptonic 1 you get
                     ! only events with one top going to an electron or positron, and
                     ! the other into any hadron.

! Parameters for the generation of spin correlations in t tbar decays
tdec/wmass 80.4  ! W mass for top decay
tdec/wwidth 2.141
tdec/bmass 4.8
tdec/twidth  1.31 ! 1.33 using PDG LO formula
tdec/elbranching 0.108
tdec/emass 0.00051
tdec/mumass 0.1057
tdec/taumass 1.777
tdec/dmass   0.100
tdec/umass   0.100
tdec/smass   0.200
tdec/cmass   1.5
tdec/sin2cabibbo 0.051
! Parameters to allow-disallow use of stored data
use-old-grid 1   ! if 1 use old grid if file pwggrids.dat is present (# 1: regenerate)
use-old-ubound 1 ! if 1 use norm of upper bounding function stored in pwgubound.dat,
                 ! if present; # 1: regenerate

ncall1 10000   ! number of calls for initializing the integration grid
itmx1 5        ! number of iterations for initializing the integration grid
ncall2 100000  ! number of calls for computing the integral and finding upper
               ! bound
itmx2 5        ! number of iterations for computing the integral and finding upper
               ! bound
foldcsi   1      ! number of folds on x integration
foldy   1      ! number of folds on y integration
foldphi 1      ! number of folds on phi integration
nubound 100000  ! number of bbarra calls to setup norm of upper bounding function
iymax 1        ! <= 10, normalization of upper bounding function in iunorm X iunorm
               !  square in y, log(m2qq)
ixmax 1        ! <= 10, normalization of upper bounding function in iunorm X iunorm
               ! square in y, log(m2qq)
```

```
xupbound 2       ! increase upper bound for radiation generation

pdfreweight 1        ! PDF reweighting
dampreweight 1       ! h_damp reweighting (0.9959*mt, 1.581*mt, mt*2.239)
storeinfo_rwgt 1     ! store weight information
withnegweights 0     ! default 0


#manyseeds 1

#parallelstage 4

#xgriditeration 1 1
```

APPENDIX B

The distributions of RPV SUSY samples produced with stop $\tilde{t}$ masses between 300 and 1000 GeV are compared with the nominal $t\bar{t}$ sample and CMS data.

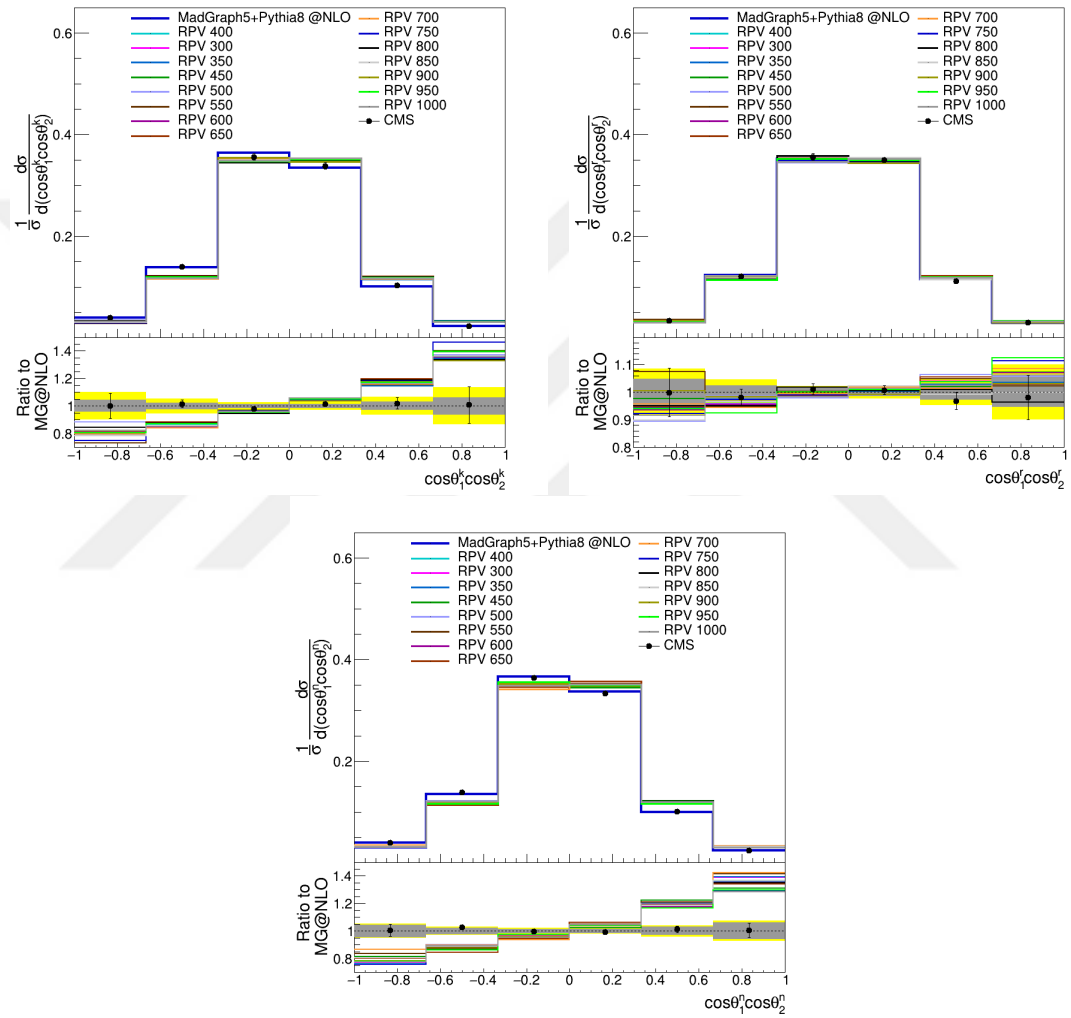

Figure B.1 : The normalized differential cross sections with respect to the diagonal spin correlation observables $\cos\theta_1^i \cos\theta_2^i$, $i = k, r, n$ compared to the nominal $t\bar{t}$ sample, the CMS data and the RPV SUSY signals with different stop $\tilde{t}$ masses. The ratio panels compare the RPV SUSY signals to the nominal distribution.

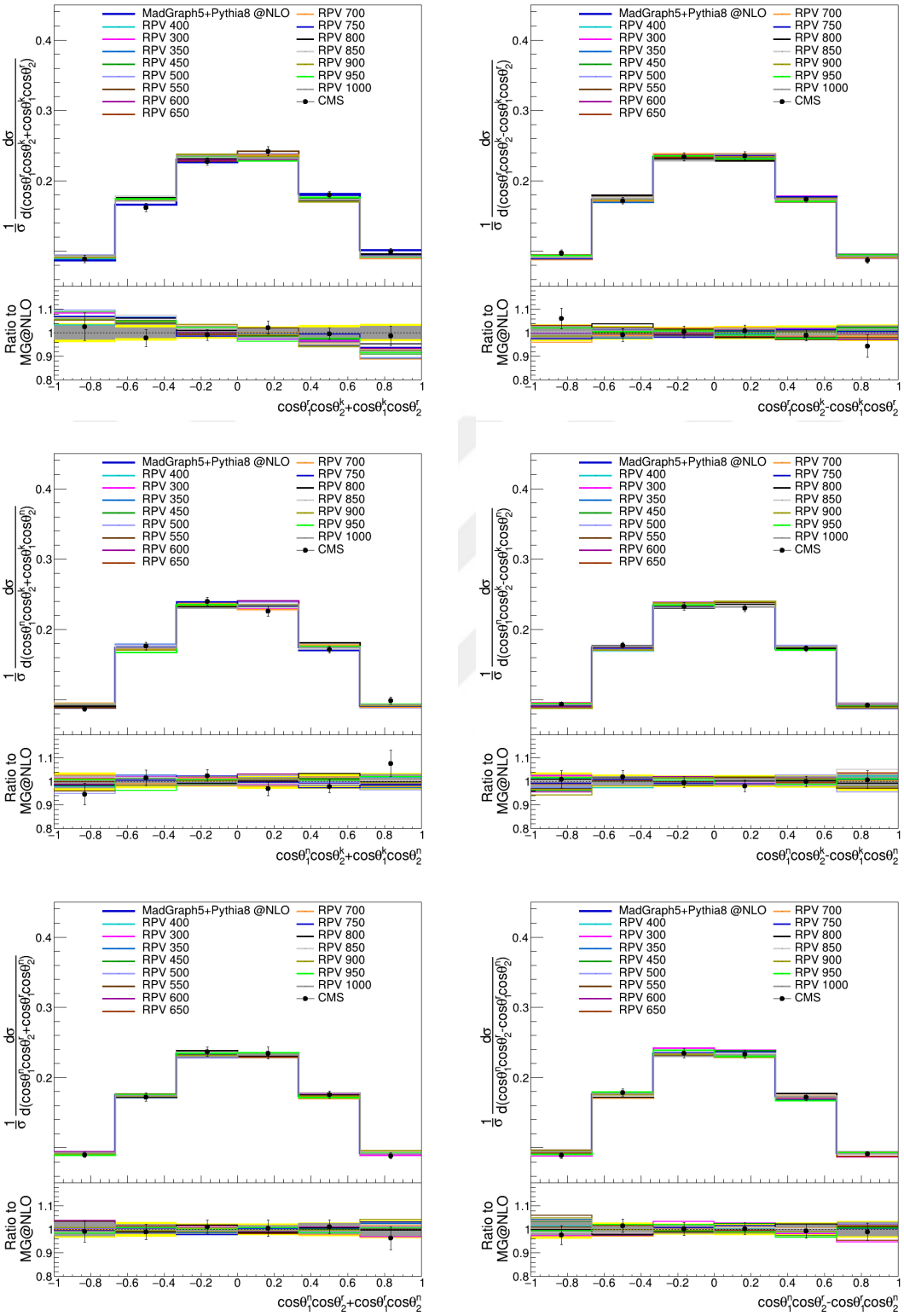

Figure B.2 : The normalized differential cross sections with respect to the cross spin correlation observables $\cos\theta_1^i \cos\theta_2^j \pm \cos\theta_1^j \cos\theta_2^i$, $i \neq j$. The ratio panels compare the RPV SUSY signals to the nominal distribution.

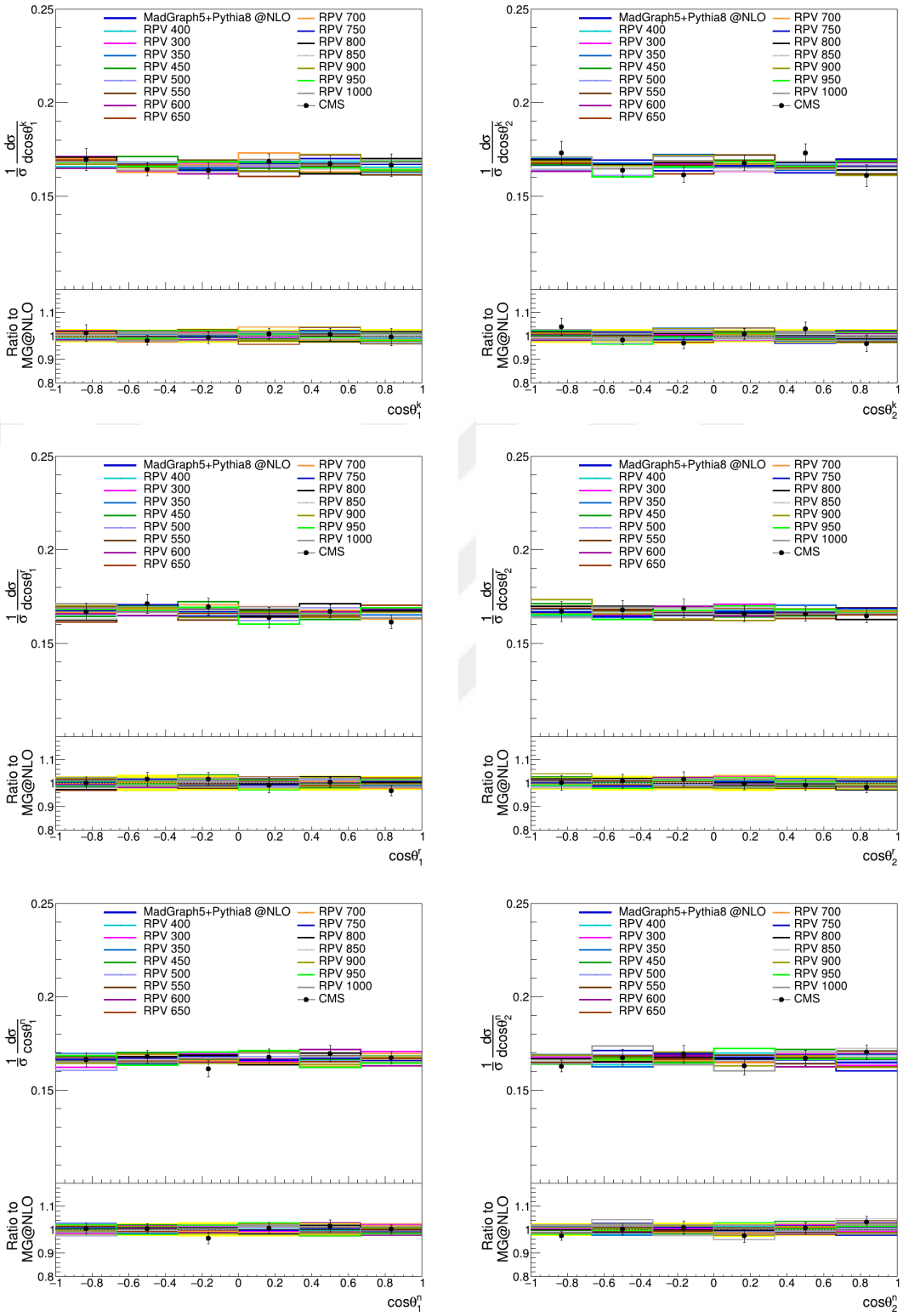

Figure B.3 : The normalized differential cross sections with respect to the observables $\cos\theta_1^i$ and $\cos\theta_2^i$, $i = k, r, n$. The ratio panels compare the RPV SUSY signals to the nominal distribution.

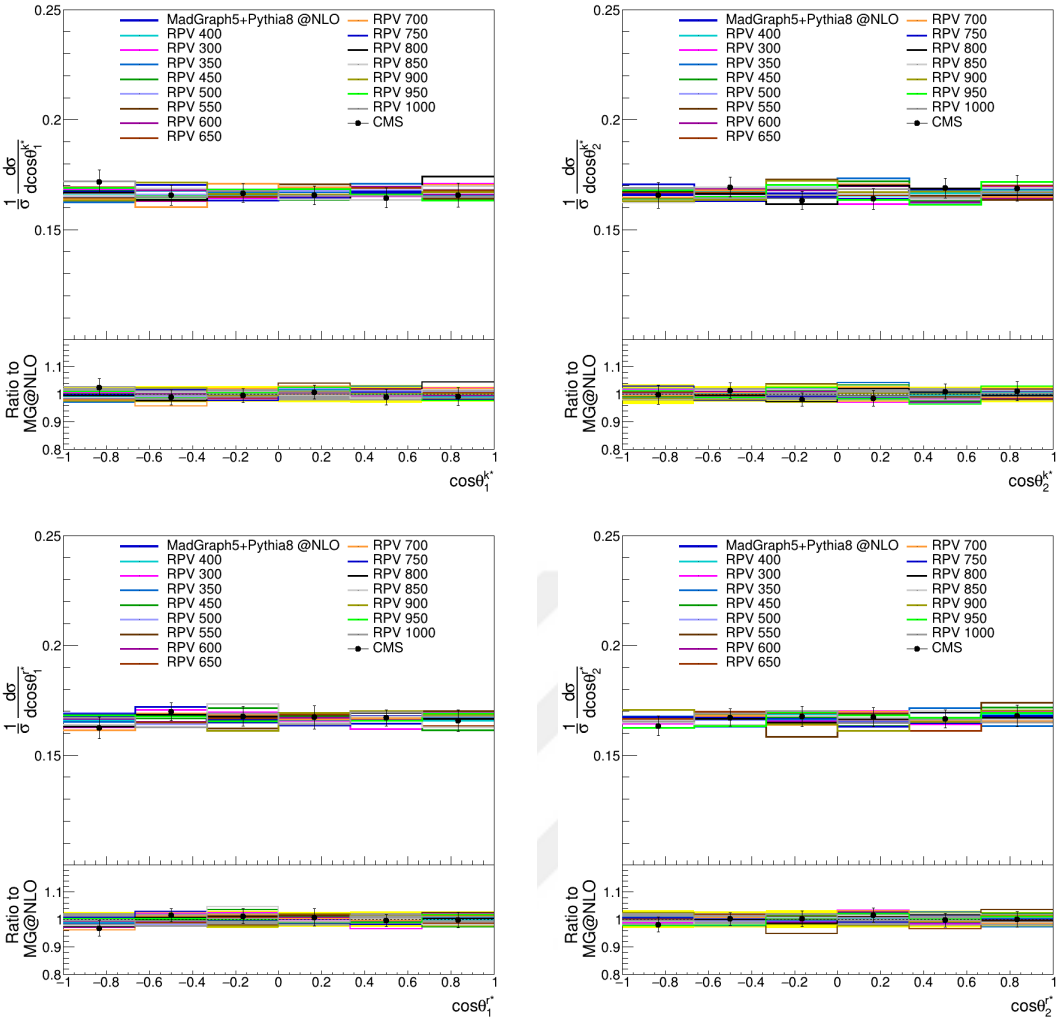

Figure B.4 : The normalized differential cross sections with respect to the observables $\cos\theta_1^{i*}$ and $\cos\theta_2^{i*}$, $i = k, r, n$. The ratio panels compare the RPV SUSY signals to the nominal distribution.

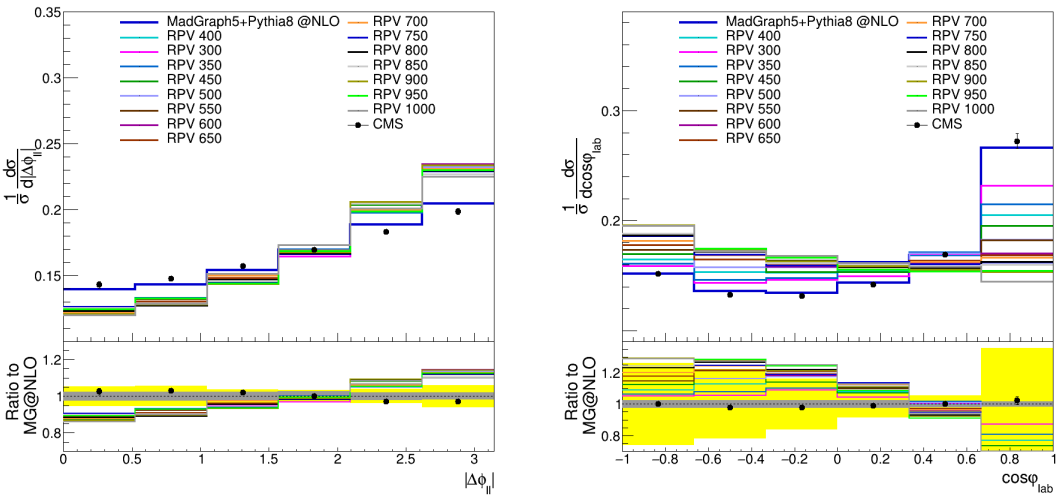

Figure B.5 : The normalized differential cross section as a function of laboratory frame observable which are $|\Delta\phi_{ll}|$ (left plot) and $\cos\varphi_{lab}$ (right plot).The ratio panels compare the RPV SUSY signals to the nominal distribution.

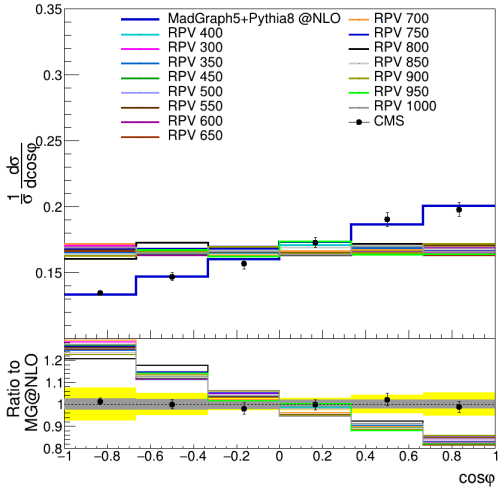

Figure B.6 : The normalized differential cross section with respect to $\cos\varphi$. The ratio panel compares the RPV SUSY signals to the nominal distribution.

CURRICULUM VITAE

Name Surname : Orçun Kolay

EDUCATION :

- **B.Sc.** : 2018, Istanbul Technical University, Faculty of Electrical and Electronics, Department of Electronics and Communication Engineering
- **M.Sc.** : 2021, Istanbul Technical University, Faculty of Science and Letters, Department of Physics Engineering

PROFESSIONAL EXPERIENCE AND REWARDS:

- 2019-2021 Research Assistant in Physics Engineering department at Istanbul Technical University